UNIVERSITÉ DE SHERBROOKE
Faculté de génie
Département de génie Mécanique

UN MODÈLE VIBROACOUSTIQUE POUR PRÉVOIR L'EFFET DE NICHE SUR LA PERTE PAR TRANSMISSION SONORE

Mémoire de maîtrise
Spécialité : Génie Mécanique

Mohammad Sadegh GHOLAMI

Jury : Noureddine ATALLA (directeur)
Franck SGARD
Raymond PANNETON

Sherbrooke (Québec) Canada March 2013

Your file Votre référence
ISBN: 978-0-494-96276-3

Our file Notre référence
ISBN: 978-0-494-96276-3

UNIVERSITÉ DE SHERBROOKE
Faculté de génie
Département de génie Mécanique

VIBRO-ACOUSTIC MODEL TO PREDICT NICHE EFFECT ON SOUND TRANSMISSION LOSS

Mémoire de maîtrise
Spécialité : Génie Mécanique

Mohammad Sadegh GHOLAMI

Jury : Noureddine ATALLA (directeur)
Franck SGARD
Raymond PANNETON

Sherbrooke (Québec) Canada March 2013

Résumé

La répétabilité et la reproductibilité sont les problèmes les plus communément rencontrés dans les études expérimentales de pertes par transmission. Des différences significatives ont été observées, dans différents laboratoires, sur des mesures de perte par transmission sonore de systèmes installés dans une niche (tunnel séparant la source des pièces réceptrices). Ces essais comparatifs inter-laboratoires ont trouvé que la perte par transmission sonore est influencée, non seulement par la plaque, la source et les paramètres récepteurs, mais aussi par la profondeur de niche et la localisation de la plaque dans celle-ci.

L'objectif principal de ce travail est de développer et de valider une méthode semi-analytique qui soit à la fois rapide, en comparaison avec les méthodes des éléments finis et des éléments de frontière, et fiable afin d'étudier l'effet de la niche sur la perte par transmission sonore. Ainsi, une méthode semi-analytique est proposée et utilisée pour investiguer l'effet de plusieurs paramètres de niche sur la perte par transmission sonore d'une fine plaque élastique. Dans cette étude, deux problèmes seront investigués. Le premier traite de la niche sans plaque dans celle-ci, appelé « aperture ». Le second traite de l'effet de la niche sur la perte par transmission sonore d'une plaque bafflée.

Les ondes acoustiques dans la niche sont développées en termes de modes acoustiques évanescents et propagatifs. Plusieurs exemples sont présentés pour étudier la convergence et valider l'approche. Les découvertes montrent une décroissance considérable dans la puissance transmise lorsque la longueur de niche augmente. De plus, la longueur de niche joue un rôle important dans la transmission sonore comparée à la surface de section transverse de celle-ci. Dans le système niche-plaque, la niche affecte le champ d'excitation en augmentant la pression sur la plaque. L'augmentation de pression est plus importante au niveau des angles et des arêtes de la plaque. Nos résultats d'étude révèlent que la niche a plus d'effet sur le champ d'excitation que sur le champ de radiation. Ceci est important pour les essais expérimentaux où le champ source est mesuré dans une chambre réverbérant. Un minimum de perte par transmission sonore, en comparaison avec d'autres positions de plaque dans la niche, est obtenu lorsque la plaque est située au centre de la niche. Par conséquent, l'effet de niche est moins important quand la plaque est située dès le début de la niche.

Mots-clés: Vibroacoustique, L'effet de niche, La perte par transmission sonore, La méthode semi-analytique, L'effet d'aperture.

Resume English

Repeatability and reproducibility are most common problems in experimental transmission loss studies. Significant differences have been seen in the measurement of sound transmission loss of systems installed in a niche (tunnel separating the source and receiving rooms) in different laboratories. These round robin tests found that sound transmission loss is influenced by not only the plate, source and receiving parameters but also by niche depth and the location of the plate within it.

The main objective of this work is to develop and validate a fast, in comparison with finite element and boundary element methods, and reliable semi-analytical method to study the effect of niche on sound transmission loss. So, a semi-analytical method is proposed and used to investigate the effect of various niche parameters on sound transmission loss of a thin elastic plate. In this study two problems will be investigated. The first deals with the niche without plate inside it which is called "aperture". The second deals with the effect of niche on sound transmission loss of baffled plate.

The acoustic waves inside the niche are expanded in terms of evanescent and propagating acoustical modes. Various examples are presented to study the convergence and to validate the approach. Findings show considerable decrease in transmitted power as the length of the niche increases. Moreover, niche's length plays more important role in sound transmission compared to its cross section area. In niche–plate system, niche affects the excitation field by increasing the pressure over the plate. This increase of pressure is more considerable at corners and edges of the plate. Our study results reveal that niche has more effect on excitation field than radiation field. This is important for experimental tests where the source field is measured in a reverberant room. Minimum sound transmission loss, in comparison with other plate position inside the niche, is obtained when the plate is placed at the center of the niche. In this case, niche affects both exciting and radiation fields and because of geometrical symmetry maximum transmission happens at this position. Consequently the niche effect is less considerable when plate is placed at the front side of the niche.

Keywords: Vibro-acoustic, Niche effect, Sound transmission loss, Semi-analytical model, Aperture effect.

Acknowledgment

It is with immense appreciation that I acknowledge the support and help of my supervisor, Professor Noureddine Atalla, for his excellent guidance, caring, patience, and providing me with an excellent atmosphere for doing research. Without his guidance and persistent help this dissertation would not have been possible.

I would like to appreciate Professor Frank Sgard and Celse Kafui Amédin whom I learned a lot from them during this study.

Table of Contents

Table of Figures

List of Tables

List of Acronyms

Technical term	Definition
BEM	Boundary Element Method
DAF	Diffuse Acoustic Field
FEM	Finite Element Method
GAUS	Group d'Acoustique de l'Université de Sherbrooke
IL	Insertion Loss
SIF	Semi-Infinite Fluid
STL	Sound Transmission Loss

List of Variables and Symbols

Symbol	Definition
a, b, d	Opening dimension and depth of the niche
B'	Complex bending stiffness
c_i	Sound velocity in each sun region
E	Young's modulus
f_c	Critical frequency of the baffled plate
h	Plate thickness
j	Imaginary number of module, $j = \sqrt{-1}$
k_0	Acoustic wave number
k_b	Bending wave number
$k_{i,pq}$	Wave number in niche 2 and 3
k_x, k_y, k_z	Wave number projections in x, y and z direction
m	Mass of the plate
p_1, p_2, p_3, p_4	Pressure in each sub region
p_b	Blocked pressure
p_{inc}	Incident pressure
p_r	Radiated pressure
p_R	Reflected pressure
S, S_1, S_2	Surface area
$u_{i,n}$	Normal velocity
v_s	Volume of the plate
$W(x, y, z)$	Displacement field
z_p	Plate position
θ, φ, r	Spherical coordinates
θ_{lim}	Limit angle
$\lambda_a, \lambda_{xy}, \lambda_z$	Acoustical wavelength, acoustical wave length in x-y plane, in z direction
ν	Poison ratio
ξ	Normalized plate position inside the niche
ρ_i	Fluid density in each sub region
τ	Transmission coefficient
τ_{diff}	Transmission coefficient in diffuse field
ω	Angular velocity rad/s

CHAPTER 1 INTRODUCTION

1.1 References

This research is done under supervision of Professor N. Atalla at "Group d'Acoustique de l'Université de Sherbrooke (GAUS)". This study is a part of wider AUTO21 funded project attempting to study the acoustical behavior of niche systems which plays an important role in noise measurements passing through baffled plate between anechoic and reverberant rooms.

1.2 Technological problem

In recent years comprehensive research, on theoretical as well as experimental basis, has been done for the airborne sound transmission through a baffled specimen. In theoretical studies, the thickness of infinite or finite baffle is assumed to be the same as thickness of finite specimen. Consequently, the baffle and specimen, i.e. plate, are coplanar, but this hypothesis is not valid any more in experimental studies. Generally, in order to create a baffle in the lab, a mounting frame (test window) made up from several layers of isolators and insulators should be installed inside the wall between reverberant and anechoic rooms. So, the test window is considerably thicker than specimen as shown in Figure 1.1. This difference in thickness affects the acoustical behaviour of the specimen when it is large compared to acoustic wave length. In addition, in this new configuration of baffle, there is the variety of specimen position. Experimental reports show that this parameter also affects the sound transmission loss (STL) measurements.

Because of these reasons different results are obtained at different test facilities, even when the same panels are tested. The term "Niche Effect" is used to refer to the discrepancies caused by the above mentioned reasons. So, niche effect is known as responsible for the inconsistency of low frequency sound transmission measurements. Another possible reason for the discrepancies is the acoustic field in reverberation room where at low frequency range, the model behaviour of room and specimen can affect the STL measurement (Vinokur, 2006). So,

such large differences in reproducibility haven't put the reliability of sound transmission loss beyond doubt.

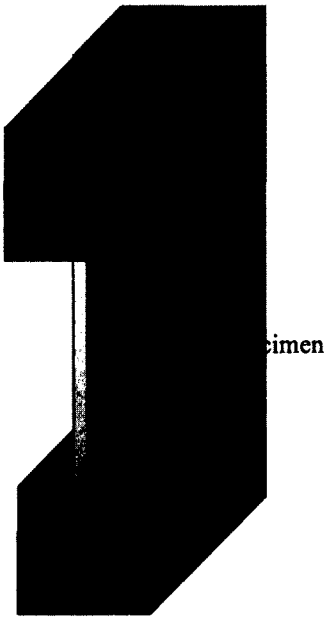

Figure 1.1: Specimen mounted inside an aperture.

Niche effect is considerable when niche with a depth comparable to the acoustic wave length behaves like an acoustic duct. Then, the pressure field inside the niche alters the structural response of the specimen. Several experimental studies (Halliwell & Warnock, 1985) and (Vinokur, 2006) reported that the difference in measured sound transmission loss of the system is related to the plate position inside the niche, Figure 1.2 . In addition other parameters such as tunnel depth and specimen size and shape affect the STL of the system.

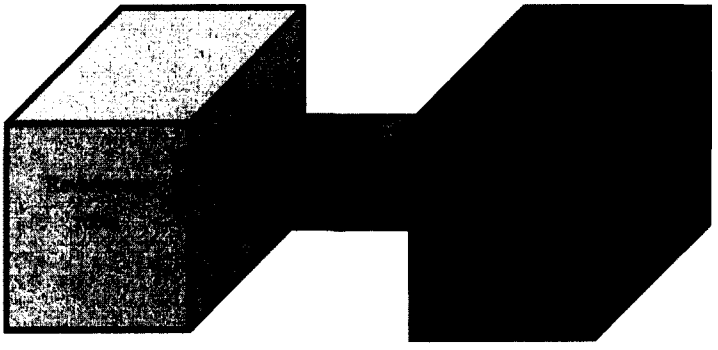

Figure 1.2: Possibility of plate position inside aperture.

1.3 Scientific problem

General numerical methods such as finite element method (FEM) or hybrid finite element-boundary element method (FEM-BEM) can be used to study the niche effect. Studying the niche effect while neglecting the effect of acoustic modes of reverberation and receiving rooms means that niche should be connected to semi-infinite fluid (SIF) on each side. The lacks of memory and calculation time problems arise when maximum frequency increases. Accordingly, the main technological objective in this work is to investigate the effect of niche and variation of sound transmission loss with the parameters of panel location, tunnel depth, and panel size using a fast, compared to FEM-BEM, semi-analytical method. Hence, the following query is the open scientific question for this study;

"What is the effect of a niche and its parameters on the sound transmission loss of a baffled panel?"

1.4 Objective

The aim of this study is to extend and validate a fast, in comparison with finite element and boundary element methods, semi analytical method to study the effect of niche on STL. Two problems will be investigated. The first deals with the niche without plate inside it, which is called "aperture". The second deals with the effect of niche on STL of baffled plate. To this end, following tasks are designed:

1.4.1 Task (I): Literature review

Conduct a literature review on previous works which are related to the topics of this work.

1.4.2 Task (II): Effect of aperture on STL

Review and validate the semi-analytical method for the niche without plate and provide the reader with numerical results regarding the effect of length and cross section area of the aperture and excitation field on STL.

1.4.3 Task (III): Effect of niche on STL of baffled plate

Propos a general and efficient semi-analytical method to predict both plane wave and diffuse acoustic field (DAF) sound transmission loss of aperture of rectangular cross section. Validate the numerical results with existing in-house code, NOVAFEM.

1.4.4 Task (IV): Effect of niche parameters on STL

Investigate the effect of niche length on STL of the plate and the effect of plate position inside the niche on STL.

1.5 Summary

In this chapter the problematic, objectives and open scientific question were introduced. In addition the main objectives of this study were detailed. As mentioned, the niche effect is associated with the difference in thickness of specimen and baffle. This effect is known as reason of difference in STL measurements in different labs with the same conditions for tests. Chapter 2 presents a review of literature on previous studies which are related to the mentioned objectives. This review shows that there is no rigorous and convincing theoretical and numerical prediction model on the effect of niches. Developing a powerful, reliable and fast, compared to FEM-BEM, semi-analytical tool to address these questions is the objective of this work. The rest of this document is organized as follows. In chapter two, a review on general numerical methods is done and then the most important experimental or numerical studies related to the topic are considered. In chapter 3, the method for niche system without plate is represented, validated and then the effect of length and cross section area of an aperture on its STL are considered. The STL of the niche-plate system is studied in chapter 4.

CHAPTER 2 LITERATURE REVIEW

2.1 Preface

Access to the theoretical or numerical prediction tools which have good compatibility with experimental results is always one of the designers demand. Although it is possible to study some acoustical behaviours such as radiation efficiency of simple acoustic systems analytically (Leppington, et al., 1982), there is no exact analytical solutions for solving baffled or unbaffled complicated structures which are excited by acoustical or mechanical time harmonic excitations (Mattei, 1995). Therefore, having numerical tools which by using them reaching to accurate and durable solutions is necessary. The major numerical methods in use are finite element method and boundary element methods. Finite element method was one of the first important numerical structural acoustic method. FEM can implement in large variety acoustic topics; from calculating nonlinear acoustic response of plates (Hwang & Pi, 1972) to composite plates with different excitation (Chen, et al., 1995). A comparison between finite element and plate theory approach was done by (Prosser, et al., 1998).

Finite element procedures are important and inseparable part of engineering analysis and design (Bathe, 2006). Finite element methods are based on variation form of structural and acoustic problems (Zienkiewicz & Taylor, 2000). A model for coupled acoustic and structural problems was introduced by (Gladwell, 1966). Some improvements, after that, are made on it (Crags, 1971a) (Crags, 1972b). Modal analysis can be done by FEM (Atalla & Bernhard, 1994). Through this method system is divided into several subsystems and the mode of each subsystem represents the response of that subsystem. To be sure about of the accuracy of response, it is necessary to have a sufficient number of modes. But FEM is not appropriate to solve acoustic problems involving infinite domains. The finite element method is not good to solve most problems on scattering and radiation involving infinite domain. Boundary integral methods are more straightforward for such problems. Boundary integral approaches can solve these kinds of problems by using surface integral involving boundary conditions and field problem (Atalla, 2011). These two methods have two disadvantages (Mattei, 1995). First, since they are completely numerical, the preparation of data is a heavy work. Second, by

increasing frequency, the computational effort increases rapidly. The boundary element method implementation in acoustic field is based on Helmholtz integral equation (Silva, 1994). This method is capable for both interior and exterior problems. Potential theory is the base of the indirect boundary element method. The coupled BEM/FEM method is applicable to solution of sound transmission or radiation problems (Seybert, et al., 1985). However, too much computation time is consumed by using this approach; this method was improved by (Tournour & Atalla, 1998) and (Ji & Sha, 1997).

2.1.1 Effect of niche

The performance of the airborne acoustic transmission is affected by the openings. The ratio of the size of the opening to acoustic wavelength is the criteria to call it as "leak" or as "opening". The small ratio refers to the former and the bigger ratio denotes to latter terms. Niche, simply, is an open cavity coupled to baffled plate. This cavity radiates inside a larger cavity or an infinite fluid. In this study, term "aperture" refers to the case in which there is no plate. The theoretical concept of sound insulation was derived for infinite baffles under free field condition on both sides (London, 1950). The acoustic field inside the aperture is assumed as summation of two plane waves propagating in opposite directions by (Sauter & Soroka, 1969) and (Wilson & Soroka, 1964). They use the radiation impedance functions of rigid massless baffled piston to account for the coupling between the aperture and the outer environment. Using the same method, STL of circular and rectangular apertures of finite thickness are studied by (Sauter & Soroka, 1969) (Wilson & Soroka, 1964), respectively. The sound field diffracted by the edges of an unbaffled circular aperture is calculated by (Furue, 1990). He also calculated the sound field radiated from a baffled rectangular aperture excited by a point source at high frequency. In order to show the effect of niche on sound transmission loss in acoustic system, a comparison between niche and simple finite plate in an infinite baffle was given by (Kim, et al., 2004), theoretically. A two dimensional system in which a finite panel was installed in a tunnel is considered. The scattering and radiation fields resulting from the tunnel were expressed by the Fourier Transform. Their study shows that STL decreases below critical frequency in comparison to the case without tunnel. This is because of the fact that tunnel is capable of increasing resonant transmission, and end reflection from

both ends of tunnel increases the pressures difference between both sides of plate, thus the plate vibration level increases. The effect of diffuse acoustic field on STL of aperture with finite thickness was studied by (Sgard, et al., 2007). The proposed method was applied for rectangular and circular cross section. Authors used the Rayleigh integral to connect the niche to the semi-infinite fluids from both sides. Using the same assumptions for niche parts but not for the exciting and receiving sides, STL of multilayered structures with thin air layers through wave based method was introduced by (Dijckmans, et al., 2010 b) and (Dijckmans & Vermeir, 2012). The method was used to predict the niche effect on STL of single and double walls inserted inside the niche. In all mentioned studies, except study which is done by (Sgard, et al., 2007) , niche is affected by the modes of source and receiving rooms.

Niche effect depends on some niche parameters such as specimen position in the aperture (Vinokur, 2006). An illustration of the geometry of the problem is given in Figure 2.1. ρ_i, c_i are the fluid density and sound speed inside the fluid, respectively. The plate is placed inside the niche.

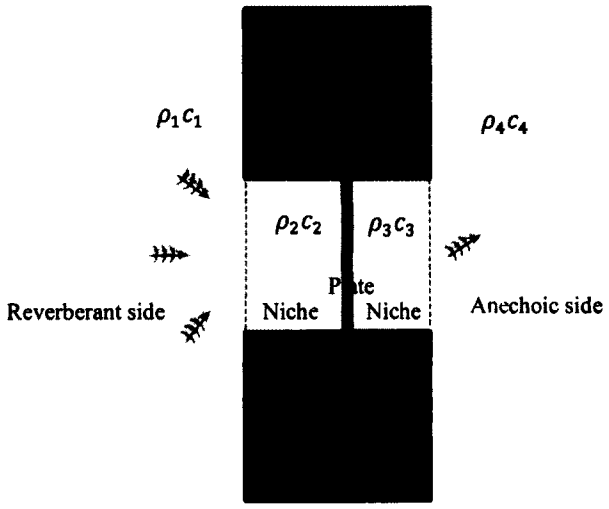

Figure 2.1: Niche and plate configuration. Plate is placed inside the niche.

2.1.2 Effect of plate location

The effect of specimen location (Figure 2.2) on STL was considered experimentally by many researchers (Halliwell & Warnock, 1985), (Vinokur, 2006) and (Cops, et al., 1987). Two ways of measurement, sound intensity techniques and conventional techniques are considered by (Halliwell & Warnock, 1985). In their experimental study for each measurement the specimen was placed in five positions inside the niche between two, anechoic and reverberant, rooms and for each position they changed the anechoic room absorption to have four different absorptive conditions. At low frequency range, the STL obtained by the former method is systematically smaller than those obtained by the latter at each position of plate. In both methods the STL was reduced when plate was placed at the center of the tunnel. These results for specimen location are confirmed by (Cops, et al., 1987), experimentally. A possible explanation could be underestimation of transmitted intensity due to the absorption of the panel. The studies of (Kim, et al., 2004) show that the sound transmission, when plate is placed at the center, increases. The difference between STL of plate when it placed at each ends or at center of the niche, is much more noticeable when the depth of tunnel increases. In addition, their findings imply that at low frequencies STL decreases when the panel displaced inside the niche, starting from front-side of the niche to the center and STL increases by shift from center to the back-side of the niche.

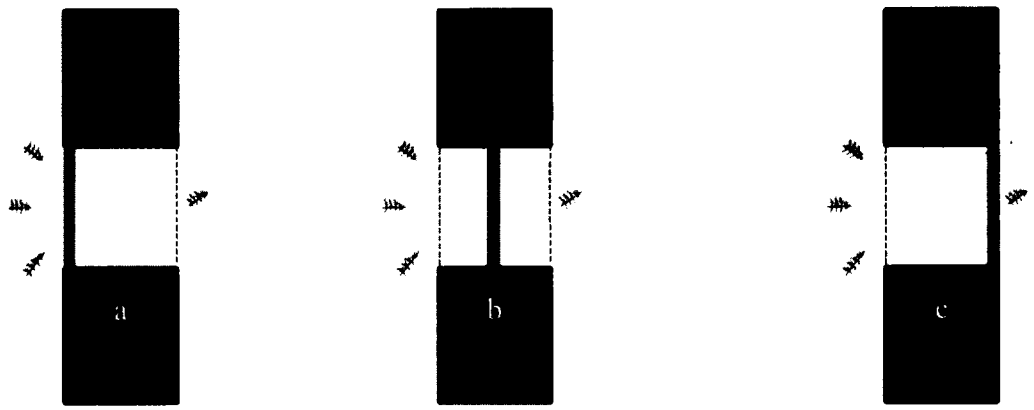

Figure 2.2: Three different position of plate inside niche; a) plate placed in front of the niche, b) Plate placed at the center, c) Plate placed in back side of the niche.

Schematic results from previous experimental studies (Kim, et al., 2004) (Vinokur, 2006) (Cops, et al., 1987) (Halliwell & Warnock, 1985) is depicted in Figure 2.3. Normalized number to show the plate position inside the niche is defined as:

$$\xi = \frac{plate\ position}{length\ of\ niche} \qquad 2.1$$

where, ξ is normalized location of the panel. Figure 2.3 indicates the sound transmission loss of niche in which the plate moves along the niche from reverberant side to anechoic side at a given frequency below the coincidence frequency. The dashed line is STL of finite plate placed in infinite baffle. Previous studies show that sound insulation, in the low-frequencies, is known to be worse for the plate placed at center than either edge of the tunnel. Niche and plate were simulated, analytically, at low frequency by (Vinokur, 2006). He showed that the transmission loss at low frequencies decreases when plate placed at the center of tunnel in comparison to each edge. All previous studies, experimental and theoretical, are in agreement with the fact that STL decreases when the specimen is at the center of the niche, in comparison with situation in which plate is flushed with each side, and this effect is more significant below coincidence frequency.

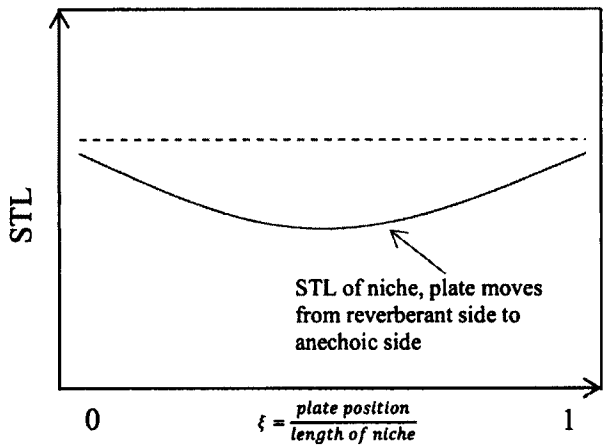

Figure 2.3: Effect of specimen position, ξ, on STL. ξ is normalized location of the panel at a given frequency below the coincidence frequency of the plate

Another experimental study done by (Kim, et al., 2004) shows that the effect of niche is more noticeable by increasing its length. An effective niche depth means the depth for wich, the

acoustical behaviour of the system is affected by niche. The definition of niche depth is shown in Figure 2.4.

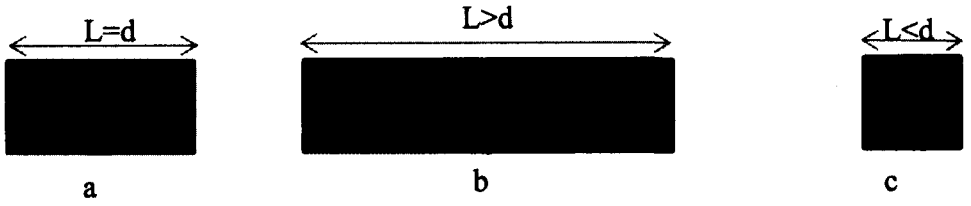

Figure 2.4: Niche depth definition for three different lengths; L is the depth and d is the depth of reference niche (a); a) normal depth, b) depth is increased, c) depth is decreased.

2.1.3 Effect of niche walls

The influence of the angled baffle on the acoustic radiation of a flat plate into a semi-infinite domain was studied analytically by (Leppington, 1996). His results indicate that the radiation resistance, with given boundary conditions, is inversely proportional to the wedge angle below the coincidence frequency. Furthermore, analytical expressions are given for the radiation efficiency of edge mode as function of angle baffle. Analytical results of Leppington were implemented by (Ohlrich & Hugin, 2004) to calculate modal-averaged correction factors. In addition, radiation efficiencies of isotropic plate were predicted and validated experimentally for different baffle angles, as shown in Figure 2.5. They, in addition, derived analytical expressions for the radiation efficiency of simply supported plate which is coplanar with infinite baffle, in which by knowing ratio of global wave numbers, ratio of acoustic medium wave number over bending wave number, and boundary constraint of the problem at hand, it is possible to read multiplication correction factor and calculate radiation efficiency of angled baffle.

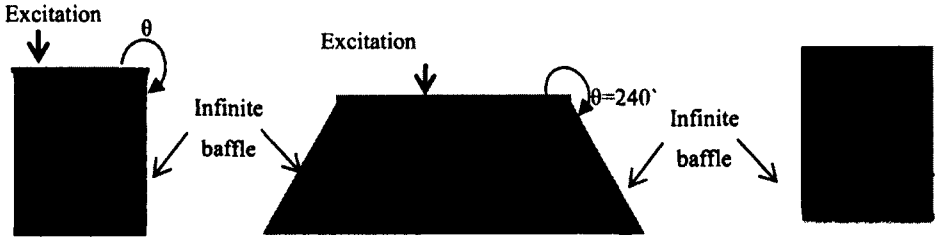

Figure 2.5: Effect of angled baffle; a) θ=270; b) θ=240; c) θ=90.

2.1.4 Effect of microphone, loudspeaker, boundary constraints and volume of rooms on STL

Effects of microphone and loudspeaker position on STL were considered by (Cops, et al., 1987). By using standard deviation for several tests, their findings show that the effects of microphone and loudspeaker position are noticeable at very low frequencies. In addition, for a plate that is placed inside a niche, below coincidence frequencies, STL increases up to 2 dB by placing a reflector plate diametrically in the opening when wave length of sound is smaller than dimension of the niche.

Having freely hinged edge condition for a plate that is going to be tested is almost impossible practically. So, there is always a difference between experimental results and theoretical ones. To solve this problem (Leppington, et al., 1983) introduced a correction factor for theoretical radiation efficiency formula of plate. They gave the radiation efficiency for edge modes when the boundary condition can be described as hinged with a rotational line-spring that resists the rotation of the plate edge. Hence, by changing the compliance the plate boundary condition can vary from clamped to simply supported edge. The effects of boundary conditions on sound radiation for baffled and unbaffled plates have been studied comprehensively in previous studies (Atalla, et al., 1996); (Xuefeng & Wen, 2010); (Yoo, 2010); (Yufeng & Qibai, 2006). They introduced new approaches for predicting sound radiation from plates with different boundary conditions. In addition their results show that the effects of boundary conditions are noticeable below coincidence frequency; and the radiation efficiency of clamped panel is 3 dB on average higher than free panels.

Results for the shape and size effect of reverberant and anechoic rooms on STL of niche show that equal volume can lead to strong coupling between them. This is the reason of STL decrease under this condition (Cops, et al., 1987). In addition they claimed that their result is valid while the shapes of rooms are equal.

2.2 Summary

In this chapter, the most important related studies have been reviewed. The most common problem in niche effect studies is repeatability. Significant differences can be seen in the sound transmission loss of the niche when measured in different laboratories. Considering the results of experimental investigation involving the round robin tests, the niche is influenced by not only the system parameters but also the exciting and receiving chambers parameter. These results show that for the same niche system, different STLs from different laboratories are obtained. So, a pure study on niche behavior and the effect of niche parameters is demanded. Niche effect is introduced as the most important reason for discrepancies between results obtained for systems which includes niche. As shown before there are experimental works on the niche effects and parameter study, in addition there is numerical study on 2D model and 3D model considering the modes of exciting and receiving rooms, but there is no numerical work considering niche parameters independent of source or receiving room conditions for 3D model.

CHAPTER 3 SOUND TRANSMISSION LOSS OF AN APERTURE

3.1 Introduction

Openings can be designed to capture engineering desires such as transferring materials or fluid flow, or they can be consequence of manufacturing or assembly process. When acoustic wavelength is much larger than the size of opening, the latter is known as "leak" while the term "opening" is used for larger dimensions (Sgard, et al., 2007). More recently, a wave based method for aperture coupled to two semi-infinite fluids was proposed by (Sgard, et al., 2007). Here, in the same way of mentioned study, the term "aperture" is used for all dimensions. In this chapter the numerical method which was presented by (Sgard, et al., 2007), to predict the sound transmission loss (STL) of an aperture with rectangular cross section, is presented. The objectives of this chapter are: first, validate our implementation in FORTRAN of the model with a GAUS written FEM/BEM code (NOVAFEM). Then, investigate the effect of aperture thickness and cross section area on STL for both plane wave and diffuse acoustic excitation.

3.2 Theory

An aperture with a finite thickness and rectangular cross section inserted into a rigid baffle and excited acoustically by oblique plane wave with incidence angles (θ_i, φ_i) as illustrated in Figure 3.1 is considered. Here θ is the angle between plane wave and z axis, and φ is the angle between the projection of acoustic plane wave into x-y plane and x axis. i, is the number of Gauss point in diffuse acoustic filed.

The region is divided into three sub-regions which are; reverberant (sub-region 1), inside aperture (sub-region 2) and receiving (sub-region 3). In Figure 3.1, k_0 is the acoustic wave number, $\{\hat{p}_1, \rho_1, c_1\}$, $\{\hat{p}_2, \rho_2, c_2\}$ and $\{\hat{p}_3, \rho_3, c_3\}$ are the pressure, density and sound velocity inside medium 1, 2 and 3, respectively. $\hat{p}_{inc}$ is the incident acoustic pressure of amplitude $\hat{A}_i$,

$\hat{p}_R$is the reflected pressure from interface between medium one and two and $\hat{p}_r$ is the radiated pressure from interface and finally the $\hat{p}_{r3}$ is the radiated pressure into medium three by back face of aperture, d is depth of aperture, $2a$ and $2b$ are dimensions of aperture in x and y direction, respectively. And finally, the origin of coordinator "o" is defined at the center of the aperture cross section.

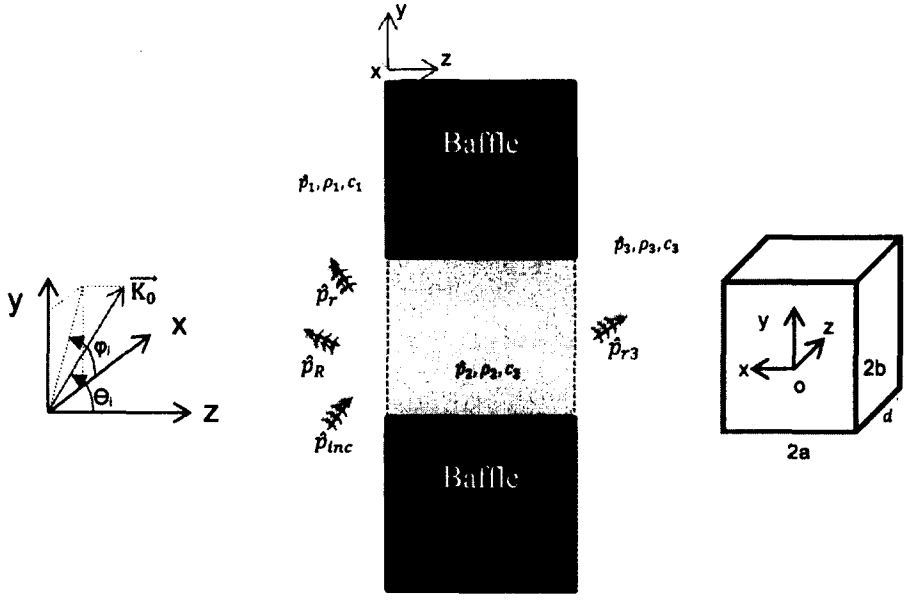

Figure 3.1: Configuration of the problem; left to right, angles of incident plane wave, pressure definition and coordinate definition.

The total acoustic field in medium one is given by

$$\hat{p}_1 = \hat{p}_{inc} + \hat{p}_R + \hat{p}_r = \hat{p}_b + \hat{p}_r \qquad 3.1$$

Where, $\hat{p}_b$ is the blocked pressure and convention $p(t) = \hat{p}e^{j\omega t}$ is used. As mentioned before the pressure in this medium consists of blocked and radiated pressure. From definition of block pressure:

$$\hat{p}_b = \hat{A}_i\, e^{-j\vec{k}.\vec{r}} + \hat{B}_i\, e^{j\vec{k}.\vec{r}} = \hat{A}_i e^{-jk_x x} e^{-jk_y y} e^{-jk_z z} + \hat{B}_i e^{-jk_x x} e^{-jk_y y} e^{jk_z z} \qquad 3.2$$

where $\hat{A}_i$ and $\hat{B}_i$ are the incident and reflected pressure amplitude, respectively. k_x, k_y, k_z are the projection of plane wave in x, y and z direction;

$$\begin{cases} k_x = k_0 \sin\theta_i \cos\varphi_i \\ k_y = k_0 \sin\theta_i \sin\varphi_i \\ k_z = k_0 \cos\theta_i \end{cases} \tag{3.3}$$

where:

$$k_0 = \frac{\omega}{c_0} \tag{3.4}$$

Here, ω is the angular frequency and c_o is the speed of sound in the air. The blocked pressure satisfies the following equation over the interface:

$$\frac{\partial \hat{p}_b}{\partial z}|_{z=0} = 0 \tag{3.5}$$

so:

$$\hat{A}_i = \hat{B}_i \text{ and } \hat{P}_b = \hat{A}_i e^{-jk_0(\sin\theta_i \cos\varphi_i x + \sin\theta_i \sin\varphi_i y)}\left(e^{-jk_z z} + e^{jk_z z}\right) \tag{3.6}$$

$$\cos(k_z z) = \frac{e^{-jk_z z} + e^{jk_z z}}{2} \tag{3.7}$$

$$\hat{p}_b = 2\hat{A}_i e^{-jk_0(\sin\theta_i \cos\varphi_i x + \sin\theta_i \sin\varphi_i y)} (\cos(zk_0 \cos\theta_i)) \tag{3.8}$$

Here $z = 0$, so:

$$\hat{p}_b = 2\hat{A}_i e^{-jk_0(\sin\theta_i \cos\varphi_i x + \sin\theta_i \sin\varphi_i y)} \tag{3.9}$$

The radiated pressure, in equation 3.1, is calculated using the Rayleigh integral over the surface $S_1 = S$ at $z = 0$. Considering the outward normal vector, $\vec{n}$, shown in Figure 3.2, the radiated pressure is written as:

$$\hat{p}_r(M) = -\int_s G(M, M_0)\frac{\partial \hat{p}_r}{\partial n}(M_0)ds \qquad 3.10$$

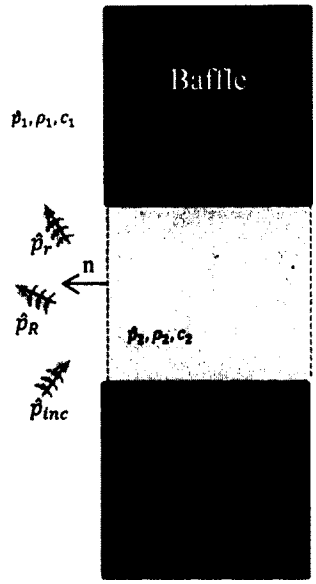

Figure 3.2: Outward normal vector definition for Rayleigh integral.

where $M$and M_o are two co-planar points at $(x, y, 0)$ and $(x_o, y_o, 0)$,

$$\frac{\partial \hat{p}_r}{\partial n} = -\frac{\partial \hat{p}_r}{\partial z} \qquad 3.11$$

and G is the baffled *Green* function given by:

$$G(M, M_0) = \frac{e^{-jk_0R}}{2\pi R} \qquad 3.12$$

$$\mathrm{R} = \sqrt{(x - x_0)^2 + (y - y_0)^2 + (z - z_0)^2} \qquad 3.13$$

The studied system consists of two interfaces which are indicated as two separate surfaces in Figure 3.3. According to the coordinate definition, two boundaries will be at $z = \{0, d\}$. Where d is the depth of niche. So, from the continuity of pressure and velocity at each interface, the boundary conditions over $S = S_1$, at $z = 0$ are:

$$\begin{cases} \hat{p}_1 = \hat{p}_2 \\ \dfrac{1}{j\omega\rho_0}\dfrac{\partial \hat{p}_r}{\partial z} = \dfrac{1}{j\omega\rho_0}\dfrac{\partial \hat{p}_2}{\partial z} \text{ or } \dfrac{\partial \hat{p}}{\partial z} = \omega^2\rho_0\,\widehat{w}_{a,i}(x,y,z) \end{cases} \quad at\ z = 0 \qquad 3.14$$

where, $\widehat{w}_{a,i}(x,y,z)$is the air particle displacement.

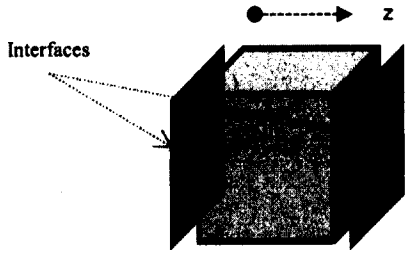

Figure 3.3: System interfaces, from left to right: interface between source & niche, niche, niche and receiving.

Thanks to boundary conditions and equation 3.10, equations 3.1 is rewritten as following;

$$\hat{p}_1 = \hat{p}_2 = \hat{p}_b + \int_s G(M, M_0)\frac{\partial \hat{p}_2}{\partial z}(M_0)ds \qquad 3.15$$

Inside the aperture (in medium two), the state acoustical pressure is governed by the homogenous Helmholtz equation:

$$\nabla^2\hat{p}_2(x,y,z) + k_0^2\,\hat{p}_2(x,y,z) = 0 \qquad 3.16$$

The acoustic pressure in medium two is approximated in terms of propagating and evanescent modes, so:

$$\hat{p}_2(x,y,z) = \sum_{p=0}^{\infty}\sum_{q=0}^{\infty}\left(\hat{A}_{2,pq}e^{-jK_{2,pq}\,z} + \hat{B}_{2,pq}e^{jK_{2,pq}z}\right)\varphi_{pq}(x,y) \qquad 3.17$$

where, $\hat{A}_{2,pq}$ and $\hat{B}_{2,pq}$ are unknown coefficients and:

$$k_{2,pq} = k_{zpq} = \sqrt{k_0^2 - \left(\frac{p\pi}{2a}\right)^2 - \left(\frac{q\pi}{2b}\right)^2} \tag{3.18}$$

$$\varphi_{pq}(x,y) = \cos\left(\frac{p\pi(x+a)}{2a}\right)\cos\left(\frac{q\pi(y+b)}{2b}\right), \qquad p,q = 0,1,2,\ldots \tag{3.19}$$

Substituting in to equation 3.17:

$$\begin{aligned} &\textstyle\sum_{pq=0}^{\infty}\left(\hat{A}_{2,pq} + \hat{B}_{2,pq}\right)\varphi_{pq}(x,y) = \\ &\hat{p}_b - j\,\textstyle\sum_{pq=0}^{\infty}\int_s\, G(M,M_0)k_{2,pq}\left(\hat{A}_{2,pq} - \hat{B}_{2,pq}\right)\varphi_{pq}(x_0,y_0)\,ds \end{aligned} \tag{3.20}$$

By multiplying by $\varphi_{uv}(x,y)$ and integrating over S:

$$\begin{aligned} &\sum_{pq=0}^{\infty}\int_s\, \varphi_{uv}(x,y)\left(\hat{A}_{2,pq} + \hat{B}_{2,pq}\right)\varphi_{pq}(x,y)\,ds \\ &\qquad = \int_s\, \varphi_{uv}(x,y)\,\hat{p}_b ds \\ &\qquad - j\sum_{pq=0}^{\infty}\int_s\,\int_s\, \varphi_{uv}(x,y)G(M,M_0)k_{2,pq}\left(\hat{A}_{2,pq}\right. \\ &\qquad \left. - \hat{B}_{2,pq}\right)\varphi_{pq}(x_0,y_0)\,dsds \end{aligned} \tag{3.21}$$

In order to simplify the equation 3.21, definitions of norm, N_{pq}^2, exciting field, $\hat{F}_{pq}$, and aperture cross modal radiation impedance, $\hat{Z}_{uvpq}$, are introduced in equations 3.22, 3.23 and 3.24, respectively;

$$N_{pq}^2 = \int_S\, \varphi_{pq}^2(x,y)ds \tag{3.22}$$

$$\hat{F}_{pq} = \int_s\, \varphi_{pq}(x,y)\,\hat{p}_b ds \tag{3.23}$$

$$\hat{Z}_{uvpq} = \frac{jZ_oK_o}{S}\int_s\,\int_s\, \varphi_{uv}(x,y)G(M,M_0)\varphi_{pq}(x_0,y_0)\,dsds \tag{3.24}$$

Here $\hat{Z}_{uvpq}$ is the aperture cross modal radiation impedance between modes (u, v) and (p, q) and Z_0 and K_0 are the characteristic impedance and wavenumber of air, respectively. For a rectangular cross section and it is given by:

$$\hat{Z}_{uvpq} = \frac{jZ_0K_0}{s}\int_{-a}^{a}\int_{-b}^{b}\int_{-a}^{a}\int_{-b}^{b}\cos\left(\frac{p\pi x}{2a}\right)\cos\left(\frac{q\pi y}{2b}\right)G(x,y,x_0y_0)\cos\left(\frac{u\pi x_0}{2a}\right)\cos\left(\frac{v\pi y_0}{2b}\right)dy_0dx_0dydx \quad 3.25$$

The quadruple integral, equation 3.24 is change into double integral and is solved via the Gauss quadrature method (Nelisse, et al., 1997); for more details see Appendix B. So, equation 3.21 can be rewritten as:

$$(\hat{A}_{2,pq} + \hat{B}_{2,pq})N_{uv}^2\delta_{uvpq} = \hat{F}_{pq} - \frac{s}{z_0k_0}\sum_{pq=0}^{\infty}k_{2,pq}(\hat{A}_{2,pq} - \hat{B}_{2,pq})\,\hat{Z}_{uvpq} \quad 3.26$$

For back side of the apertures, medium three, the radiated pressure is obtained by implementing the Rayleigh integral over the backside surface:

$$\hat{p}_3(M) = -\int_{S_2} G(M, M_0)\frac{\partial\hat{p}_3}{\partial n}(M_0)\,ds_2 \quad and \quad \frac{\partial\hat{p}_3}{\partial n} = \frac{\partial\hat{p}_3}{\partial z} \quad 3.27$$

The boundary conditions over $S = S_2$ at $z = d$ are:

$$\begin{cases} \hat{p}_2 = \hat{p}_3 \\ \dfrac{1}{j\omega\rho_0}\dfrac{\partial\hat{p}_2}{\partial z} = \dfrac{1}{j\omega\rho_0}\dfrac{\partial\hat{p}_3}{\partial z} \text{ or } \dfrac{\partial\hat{p}}{\partial z} = \omega^2\rho_0\,\hat{w}_{a,i}(x,y,z) \end{cases}^{at\ z=d} \quad 3.28$$

Using these boundary conditions and equation 3.27:

$$\hat{p}_3 = \hat{p}_2 = -\int_S G(M, M_0)\frac{\partial\hat{p}_2}{\partial z}(M_0)\,ds \quad 3.29$$

By substituting equations 3.17 and 3.28 into equation 3.29 :

$$\sum_{pq=0}^{\infty}\left(\hat{A}_{2,pq}e^{-jK_{2,pq}\,d}+\hat{B}_{2,pq}e^{jK_{2,pq}d}\right)\varphi_{pq}(x,y)$$
$$=j\sum_{pq=0}^{\infty}\int_{s}k_{2,pq}\left(\hat{A}_{2,pq}e^{-jK_{2,pq}\,d}-\hat{B}_{2,pq}e^{jK_{2,pq}d}\right)\varphi_{pq}(x_0,y_0)\,G(M,M_0)ds \tag{3.30}$$

and multiplying to $\varphi_{uv}(x,y)$, integrating over S:

$$\sum_{pq=0}^{\infty}\int_{s}\varphi_{uv}(x,y)\left(\hat{A}_{2,pq}e^{-jK_{2,pq}\,d}+\hat{B}_{2,pq}e^{jK_{2,pq}d}\right)\varphi_{pq}(x,y)\;ds$$
$$=j\sum_{pq=0}^{\infty}\int_{s}\int_{s}\varphi_{uv}(x,y)k_{2,pq}\left(\hat{A}_{2,pq}e^{-jK_{2,pq}\,d}-\hat{B}_{2,pq}e^{jK_{2,pq}d}\right)\varphi_{pq}(x,y)\,G(M,M_0)dsds \tag{3.31}$$

Using the definition of norm and cross modal radiation impedance, equation 3.31 is rephrased as:

$$\left(\hat{A}_{2,pq}e^{-jK_{2,pq}\,d}+\hat{B}_{2,pq}e^{jK_{2,pq}d}\right)N_{uv}^{2}\delta_{uvpq}$$
$$=\frac{s}{z_0k_0}\sum_{pq=0}^{\infty}k_{2,pq}\left(\hat{A}_{2,pq}e^{-jK_{2,pq}\,d}-\hat{B}_{2,pq}e^{jK_{2,pq}d}\right)\hat{Z}_{uvpq} \tag{3.32}$$

Equations 3.26 and 3.32 are cast in matrix format to calculate the unknown vectors, $\hat{A}_{2,pq}$ and $\hat{B}_{2,pq}$.

$$\begin{bmatrix}\xi_1 & \xi_2\\ \xi_3 & \xi_4\end{bmatrix}\begin{Bmatrix}[\hat{A}_{2,pq}]\\ [\hat{B}_{2,pq}]\end{Bmatrix}=\begin{Bmatrix}[\hat{F}_{pq}]\\ [0]\end{Bmatrix} \tag{3.33}$$

where, $\{\xi_i\}$ are sub-matrices defined as follows:

$$\xi_{1,uvpq} = N_{uv}^2 \delta_{uvpq} + \frac{S}{Z_0 K_0} \sum_{pq=0}^{\infty} k_{2,pq} \hat{Z}_{uvpq} \quad 3.34$$

$$\xi_{2,uvpq} = N_{uv}^2 \delta_{uvpq} - \frac{S}{Z_0 K_0} \sum_{pq=0}^{\infty} k_{2,pq} \hat{Z}_{uvpq} \quad 3.35$$

$$\xi_{3,uvpq} = e^{-jK_{2,pq}\, d}\, N_{uv}^2 \delta_{uvpq} - \frac{S}{Z_0 K_0} \sum_{pq=0}^{\infty} k_{2,pq} \hat{Z}_{uvpq}\, e^{-jK_{2,pq}\, d} \quad 3.36$$

$$\xi_{4,uvpq} = e^{jK_{2,pq}\, d}\, N_{uv}^2 \delta_{uvpq} + \frac{S}{Z_0 K_0} \sum_{pq=0}^{\infty} k_{2,pq} \hat{Z}_{uvpq}\, e^{jK_{2,pq}\, d} \quad 3.37$$

The rank of general matrix, and sub matrices are defined in the following:

$$h = 4 \times (p_{max} + 1) \times (q_{max} + 1) \quad 3.38$$

where $\{p_{max}, q_{max}\}$ are the maximum number of kept mode in $\{x, y\}$ direction for niche.

3.2.1 Calculation of vibro-acoustic indicators

Thanks to Prof. Sgard's subroutines, the equation 3.33 is implemented in a FORTRAN code and solved for a given incident oblique plane wave and diffuse acoustic field, using the linear algebra package "LAPACK". The output of the solver is two unknown vectors, $\hat{A}_{2,pq}$ and $\hat{B}_{2,pq}$, which are coefficients of pressure distribution inside the aperture, equation 3.17.

Transmitted acoustic power for one oblique plane wave is calculated as follows:

$$\begin{aligned} \Pi_t(\theta_i, \varphi_i) &= \tfrac{1}{2} Re\left[\int_s \hat{p}_3 u_{3,n}^* ds\right] = \\ &\tfrac{1}{2} Re\left[\tfrac{j}{\rho_0 \omega} \int_s \sum_{pq=0}^{\infty} \left(\hat{A}_{2,pq} e^{-jK_{2,pq}\, d} + \right.\right. \\ &\left. \hat{B}_{2,pq} e^{jK_{2,pq} d}\right) \varphi_{pq}(x,y) \sum_{mn=0}^{\infty} K^*_{2,mn} \left(-\hat{A}_{2,mn} e^{-jK_{2,mn}\, d} + \right. \\ &\left.\left. \hat{B}_{2,mn} e^{jK_{2,mn} d}\right)^* \varphi_{mn}(x,y)\, ds\right] = \tfrac{1}{2} Re\left[\tfrac{-1}{\rho\omega}\, \hat{D}_{pq} N_{pq}^2\, K^*_{2,pq} \hat{E}^*_{pq}\right] \end{aligned} \quad 3.39$$

where $u_{3,n}^*$ is the complex conjugate of normal velocity over the interface and:

$$\hat{D}_{pq} = \hat{A}_{2,pq} e^{-jK_{2,pq}\, d} + \hat{B}_{2,pq} e^{jK_{3,pq} d} \tag{3.40}$$

$$\hat{E}_{pq} = -\hat{A}_{2,pq} e^{-jK_{2,pq}\, d} + \hat{B}_{2,pq} e^{jK_{2,pq} d} \tag{3.41}$$

The incidence power is given by (Fahy & Gardonio, 2007):

$$\Pi_{inc}(\theta_i, \varphi_i) = \frac{|A_i|^2 \cos\theta_i S}{2\rho_0 c_0} \tag{3.42}$$

Whit respect to power incident and transmitted power, the oblique incidence transmission coefficient, $\tau(\theta_i, \varphi_i)$ is calculated:

$$\tau(\theta_i, \varphi_i) = \frac{\Pi_t\,(\theta_i, \varphi_i)}{\Pi_{inc}\,(\theta_i, \varphi_i)} \tag{3.43}$$

Finally the STL can be calculated as:

$$STL = -10 \log \tau \tag{3.44}$$

3.2.2 Transmitted power for diffuse acoustic field

Since there are more than one plane wave in diffuse acoustic field, the unknown coefficient vectors and exciting force sub-matrices are changed as follows:

$$\begin{bmatrix} \xi_1 & \xi_2 \\ \xi_3 & \xi_4 \end{bmatrix}_{h\times h} \begin{Bmatrix} \hat{A}_{2,pq} & \cdots & \hat{A}'_{2,pq} \\ \hat{B}_{2,pq} & \cdots & \hat{B}'_{2,pq} \end{Bmatrix}_{h\times k} = \begin{Bmatrix} \hat{F}_{pq} & \cdots & \hat{F}'_{pq} \\ 0 & \cdots & 0 \end{Bmatrix}_{h\times k} \tag{3.45}$$

where h is defined in equation 3.38 and k is:

$$k = number\ of\ Gauss\ points\ across\ \theta \times number\ of\ Gauss\ points\ across\ \varphi \tag{3.46}$$

Here, $\hat{A}'_{2,pq}$, $\hat{B}'_{2,pq}$ are unknowns associated to i^{th} plane wave and $\hat{F}'_{pq}$ is the exciting force associated from that plane wave. Plane wave Transmission coefficient is calculated as following:

$$\tau_{diff} = \frac{\int_0^{2\pi} \int_0^{\theta_{lim}} \tau(\theta_i, \varphi_i) \sin\theta_i \cos\theta_i \, d\theta d\varphi}{\pi \sin^2 \theta_{\text{lim}}} \quad 3.47$$

where $\tau(\theta_i, \varphi_i)$ is the transmission coefficient for each plane wave and

$$\theta_{lim} = 78° \left(\frac{\pi}{180}\right) \quad 3.48$$

The transmission loss is calculated as following.

$$STL = -10 \log \tau \quad 3.49$$

3.3 Numerical examples

In order to validate the proposed model and FORTRAN code, several examples are considered, the results are compared with NOVAFEM. The convergence of acoustic indicators, sound transmission loss and radiation efficiency, has been studied by looking at discrepancies as the number of modes increases. First, the convergence of the proposed model is investigated by focusing on transmission loss and on truncation frequency which is directly related to the number of modes kept in the modal expansion. Second, results are compared with results obtained by hybrid finite element method-boundary element method (FEM-BEM) for different excitation types.

3.3.1 Convergence of the approach

Aperture dimensions, fluid density and speed of sound inside the fluid and frequency interval are given in Table 3.1.

Table 3.1: Characteristics of aperture

$2a \times 2b \times d$ (m)	ρ_0 (kg/m3)	C_0 (m/s)	Frequency range (Hz)
0.4 × 0.2 × 0.05	1.213	342.2	10- 2000

As mentioned before, the number of modes plays important role in presented method. So, the effect of number of modes on sound STL is studied. Excitation parameters for both plane wave and diffuse field are detailed in Table 3.2.

Table 3.2: Excitation field characteristics

Pressure amp.	Frequency	Plane wave		Diffuse acoustic field		
A_i (pa)	f_{min}- f_{max}(Hz)	θ	φ	Number of Gauss points in θ	Number of Gauss points in φ	θ_{lim}
1	10- 2000	45°	60°	20	20	78°

The STL difference between two truncation frequencies, f_{max} and $2f_{max}$, is shown in Figure 3.4. Keeping modes up to the maximum frequency is good enough to capture the physics of the problem. The maximum difference between these two solutions is less than 0.16 dB for the frequency range and plane wave excitation. So, with respect to this result and minimum acoustic wave length and lateral size of the aperture, in this chapter, modes up to f_{max} will be retained in the modal expansion.

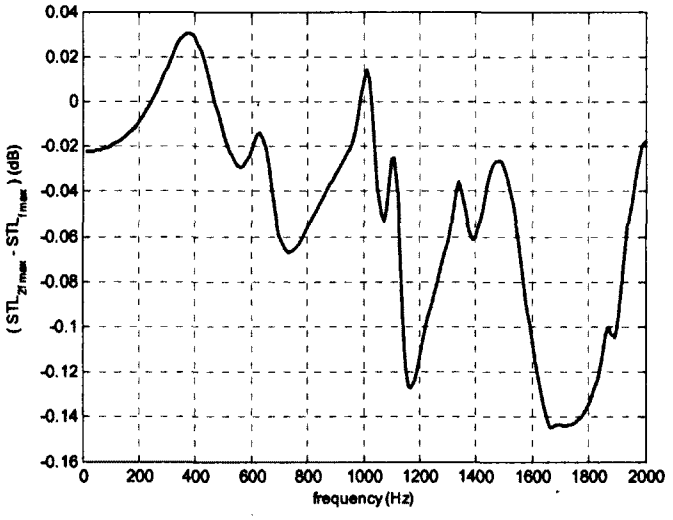

Figure 3.4: Convergence study, the effect of keeping modes up to two times of truncation frequency.

3.4 Numerical validation

In this section the results obtained from presented method are validated by the results obtained by NOVAFEM. The aperture is modeled in FEMAP as shown in Figure 3.3. The aperture volume is discretized using acoustic brick (Hexa 8) elements. Coupling with the source and receiver semi-infinite fluid is taken into account with a Rayleigh integral based impedance radiation matrix implemented within NOVAFEM (Sgard, et al., 2007). Since the convergence is slow (see Figure 4.7), 10 elements per acoustic wave length, λ_a is considered here. Number of the elements in each direction is given in Table 3.3.

Table 3.3: Number of elements for the aperture modeled in NOVAFEM

Direction	2a	2b	d
Number of Elements	30	20	4

$$\lambda_a = \frac{c_0}{f_{max}} \approx 0.18\ (m) \qquad 3.50$$

Two examples are considered here; the first, system is excited by a normal incident plane wave. Sound transmission loss of the system obtained by FEM-BEM method through NOVAFEM and proposed method is shown in Figure 3.5. In this figure a_{eq} is $\sqrt{4ab/\pi}$. The second, the STL of the aperture excited by an oblique incidence plane wave with the parameters mentioned in Table 3.2 is shown in Figure 3.6 .

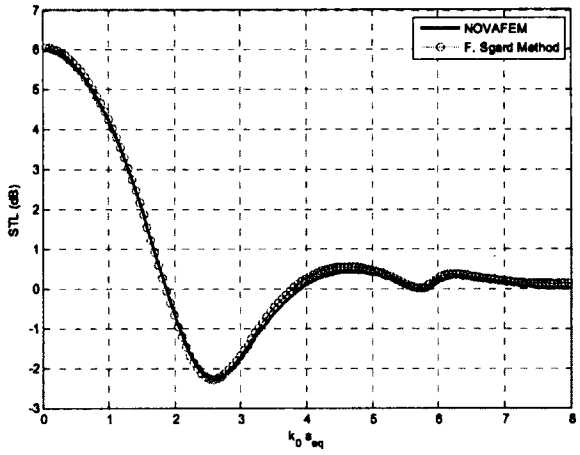

Figure 3.5: Comparison of presented method and FEM-BEM. Normal incident ($\theta_i = 0^\circ$,$\varphi_i = 0^\circ$) transmission loss of rectangular aperture (b/a=1/2, d/a=1).

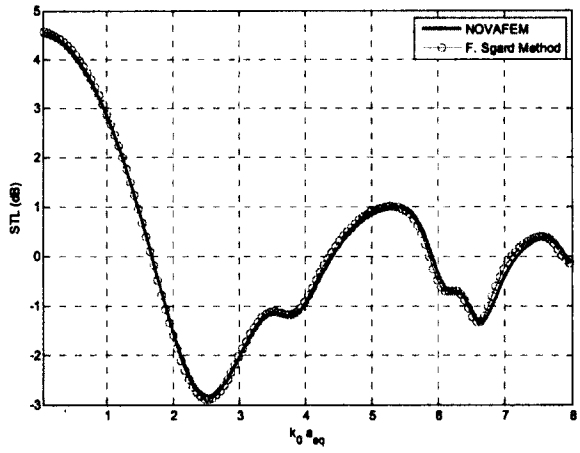

Figure 3.6: Comparison of presented method and FEM-BEM. Oblique incident ($\theta_i = 45°, \varphi_i = 60°$) transmission loss of rectangular aperture (b/a=1/2, d/a=1).

As shown in these figures, there is an excellent agreement between the proposed approach and FEM-BEM model. The effect of aperture length on STL will be studied in next section by using the proposed method.

3.5 Aperture depth and shape effect on STL

Effect of aperture depth on STL for two kinds of excitations, oblique plane wave and diffuse acoustic filed as explained in Table 3.2, is investigated here. The ratio of cross section dimensions is b/a=0.5. Several ratios of aperture depth to larger dimension, a, are considered as d/a= 0.25, d/a = 0.5, d/a = 1 and finally d/a=1.5. The results are given in Figure 3.7 for the plane wave case and in Figure 3.8 for the diffuse acoustic field. It is observed that the aperture effect is considerable up to ($k_0\, a_{eq} \cong 4$). The effect of aperture is negligible ($STL < 1\ dB$) where $k_0\, a_{eq} > 4$. The transmission loss at high frequencies converges to 0 dB which means the aperture effect vanishes when acoustic wavelength becomes smaller than niche length while at low frequencies it increases as the aperture length is increased. It means that the transmission coefficient is 1 at high frequencies; in the other words, the aperture effect vanishes when the acoustic wave length is small enough to neglect the diffraction effect.

For apertures with larger depth, d/a > 0.5, the transmission loss shows resonant behaviour. In addition, by doubling the depth ratio, d/a, STL increases about 2 dB before the first transverse mode for both type of excitations, plane wave or diffuse acoustic field. This means increasing the length up to two times will cause 60% reduction in transmitted power caused by first mode. Effect of increasing the depth up to two and three times of d/a=0.5 is shown in Figure 3.9.

Effect of excitation field, diffuse or plane wave, is shown in Figure 3.10 for two apertures with different depth. As shown in this figure the effect of diffuse field, Table 3.2, is less than 1 dB for all frequency range. The same result is obtained when the depth increase up to two times. The STL difference for both cases is less than 1 dB for all frequency range.

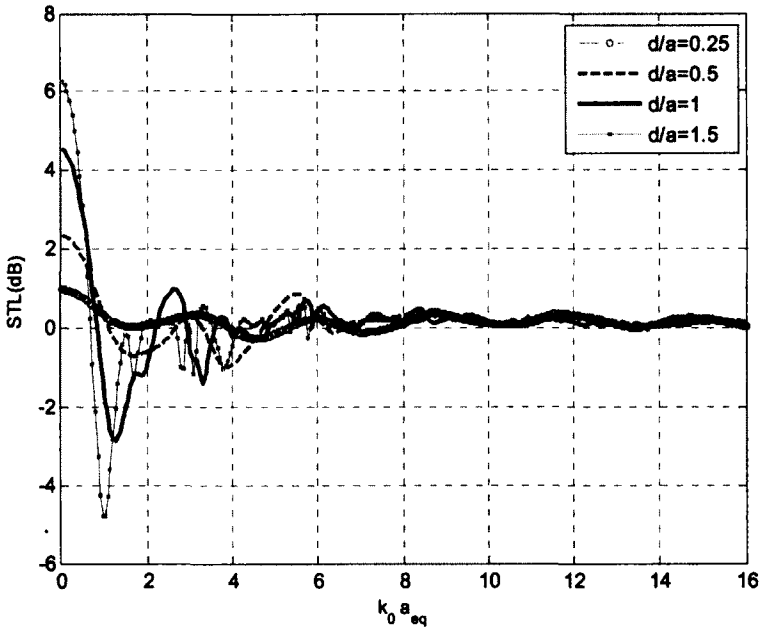

Figure 3.7: Effect of niche-depth on STL under plane wave excitation field.

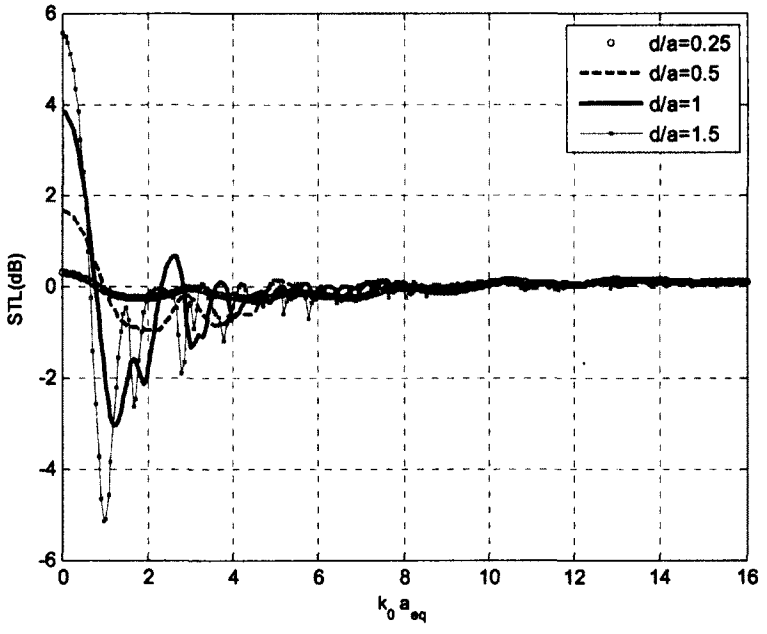

Figure 3.8: Effect of niche-depth on STL under DAF excitation field.

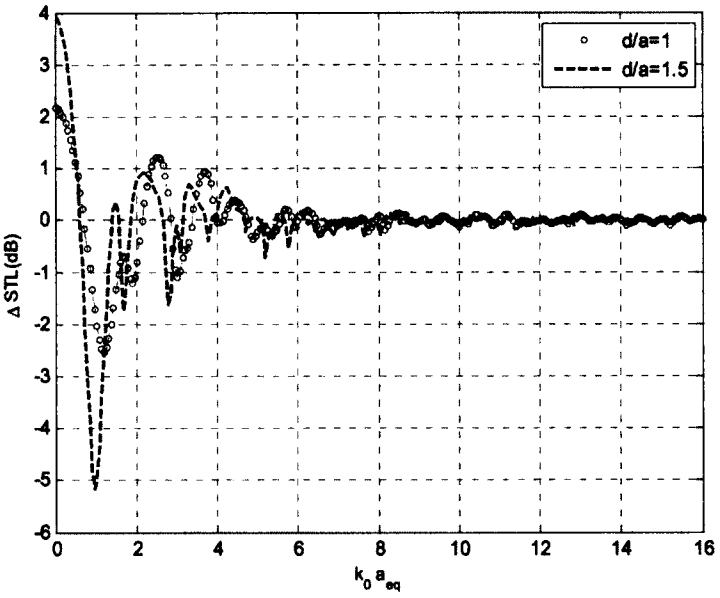

Figure 3.9: Effect of increasing the depth up to two and three times under plane wave excitation. The reference system depth is d/a=0.5.

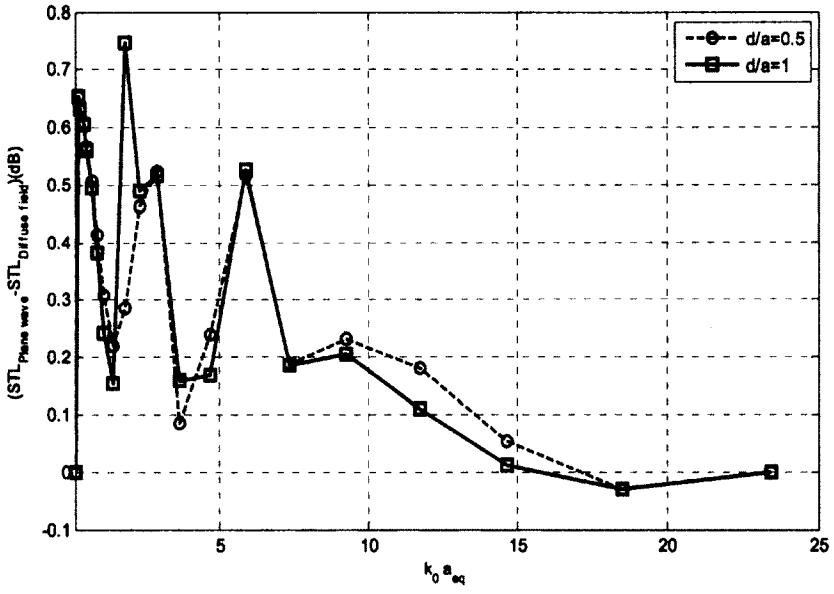

Figure 3.10: Effect of excitation field on STL shown in 1/3 octave band.

In the following, different cross section areas, the square ($b/a = 1$), and two other rectangular, $b/a = 1/2$ and $b/a = 1/3$ are studied. The area of second and third systems are two and three times of square cross section. As shown in Figure 3.11 transmission loss decreases as the geometric area increases. It should be noted that negative values of STL indicate a transmission coefficient graeter than unity which is the case for a perfectly transmitting aperture; in this situation, as (A. Sauter and W. W. Soroka) says this phenomenan is because of aperture resonace as opened tube. The amplitude of flactuations between positive and negative values reduces and eventually, the STL converged to zero. Results of increasing the area, Figure 3.11 are compared to the findings of increasing the depth, Figure 3.9. Consequently, the effect of increasing of depth on STL is more considerable than effect of increasing the area.

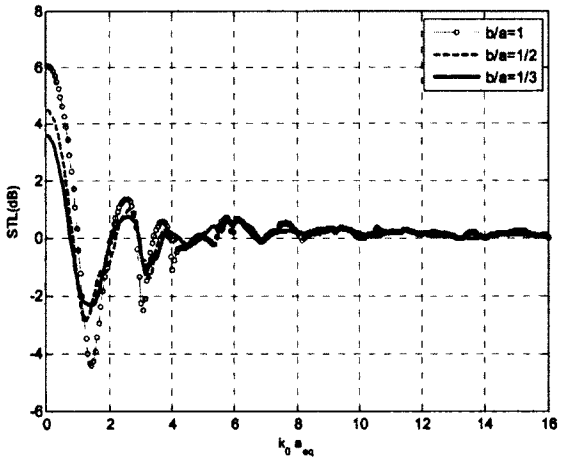

Figure 3.11: Effect of cross section area on STL.

3.6 Summary

A general numerical method, which was developed by (Sgard, et al., 2007), to study the sound transmission loss of baffled aperture of rectangular cross section is represented in this chapter. The acoustic waves inside the aperture are expanded in terms of evanescent and propagating acoustical modes. The represented method is simple, efficient and in comparison to FEM/BEM methods is fast. Various examples have been presented to study the convergence. The approach is validated by existing in-house written code NOVAFEM for rectangular cross section aperture. Outcomes imply that keeping modes up to the maximum frequency of interest suffices to capture the physics and enough robust to have convergence. The effect of excitation field (Sgard, et al., 2007), diffuse or plane waves, and aperture depth have been modeled. Findings show that, the difference between diffuse acoustic field and oblique plane wave excitation for same aperture depth is less than 1 dB at low frequencies ($k_o a_{eq} < 0.3$). In addition, 60% decrease in transmitted power is obtained when the length of the niche was doubled. Importantly, increasing in aperture depth can modify STL more considerably than reducing the cross section area.

CHAPTER 4 TRANSMISSION LOSS OF NICHE AND PLATE

4.1 Introduction

Repeatability is one of the most important issues in sound insulation measurements. There are significant differences in experimental studies on niche sound transmission loss measurements in different laboratories (Halliwell & Warnock, 1985), (Cops, et al., 1987) and (Vinokur, 2006). The results of the round robin tests show that the STL is not influenced only by the plate parameters but also by the parameters of the test environment (set up). These results confirm that for the same niche system, different STLs from different laboratories are obtained. The non-negligible differences in reproducibility haven't put the measurement results beyond doubt. In order to answer the repeatability and reproducibility question, theoretical approaches have been proposed (Leppington, 1996) (Vinokur, 2006). The STL of multilayered structures placed inside the niche while source and receiving rooms considered as closed cavities investigated using a wave based methodology by (Dijckmans & Vermeir, 2010 a), (Dijckmans, et al., 2010 b) and (Dijckmans & Vermeir, 2012). The model takes into account the full coupling between the room modes, the niche modes and the bending wave modes of the plate. In this model, niche is affected by source and receiving modes at both sides of the niche which happens in practice to. They did a parametric study for single and double walls. Their results show that the position of the plate placed inside the niche can significantly influence the STL below coincidence. They also observed that the STL of single and double walls is minimal when placed in the center of the niche and maximal for the edge positions. In addition, they showed that the niche effect is more considerable for double walls in the in mid-frequency range and STL is highly dependent on the angle of incidence in this range.

In this chapter, the effect of niche on STL of the thin plate is studied. The plate is inserted inside the niche connecting two semi-infinite fluids. The wave based method presented in previous chapter is extended to include the plate. Source and receiving side are considered as

semi-infinite fluids. Rayleigh integral is implemented for radiating pressure into each of SIFs. In this way it will be possible to study the effect of niche parameters on STL of the plate neglecting the effect of source and receiving room shape, size and modes.

First, niche and its subsystems are introduced. Then governing equations of each subsystem, starting from excitation side to receiver side, are presented. After that, subsystems are coupled to their neighbour subsystems by using the boundary conditions. Next, the system is numerically solved using the Rayleigh-Ritz method. The convergence of the used modal series is studied using various vibroacoustic indicators. To validate the method, the results obtained through the proposed method are compared with the results obtained through FEM-BEM method by modeling system in NOVAFEM. Finally, a niche parameters study is done and the results are discussed.

4.2 Theory

System consists of a plate inside a niche separating two semi-infinite fluids; both sides of the niche are baffled, as shown in Figure 4.1. When the plate is not flush mounted at either side of the niche, the system can be subdivided into five subsystems:

1. Source side (medium 1), which is a semi-infinite fluid.
2. Niche, which is placed at the left side of the plate (medium 2). It will be omitted if plate is flush mounted in the source side baffle.
3. Plate, which is considered acoustically thin.
4. Niche which is placed at the other side of the plate (medium 3). It will be omitted if plate is flush mounted in the receiver side baffle.
5. Receiver side (medium 4), which is a semi-infinite fluid.

In Figure 4.1, k_o is the acoustic wave number , $\{\hat{p}_1, \rho_1, c_1\}$, $\{\hat{p}_2, \rho_2, c_2\}$, $\{\hat{p}_3, \rho_3, c_3\}$ and $\hat{p}_4, \rho_4, c_4\}$ are the pressure, density and sound velocity inside medium 1, 2, 3 and 4, respectively. $\hat{p}_{inc}$ is the incident acoustic pressure of amplitude $\hat{A}_i$, $\hat{p}_R$ is the reflected pressure from interface between medium 1 and 2, $\hat{p}_r$ is the radiated pressure into the source side and $\hat{p}_{r4}$ is the radiated pressure into receiver medium; Here θ is the angle between plane wave and z axis, and φ is the angle between the projection of k_o into $x-y$ plane and x axis. i, refers to the particular number of plane wave composing the diffuse acoustic filed. Dimensions of niche

are $2a$, $2b$ and d in x, y and z direction, o is the center of coordinates and z_p gives the location of the plate inside the niche. $\vec{n}$ is the outward normal vector of each side of the niche.

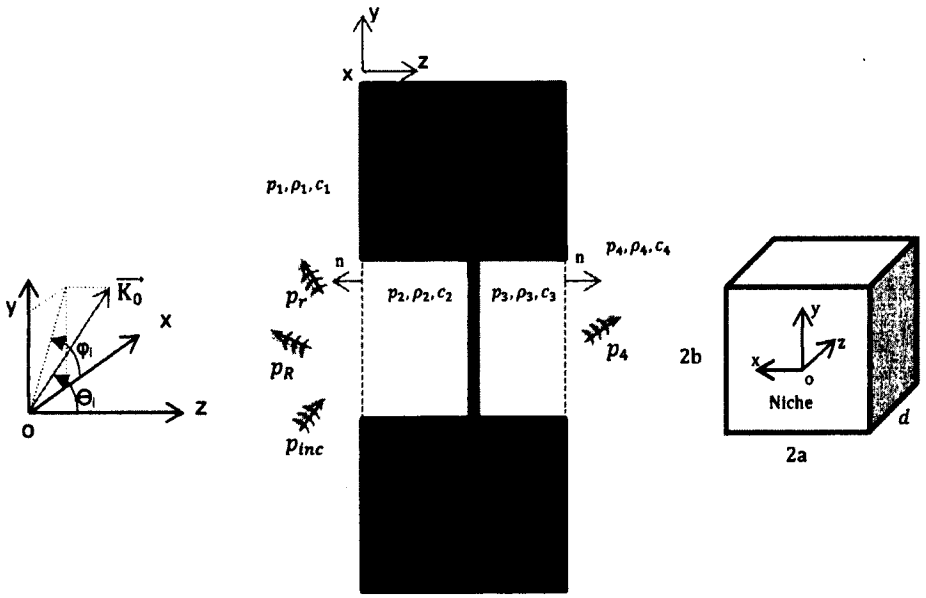

Figure 4.1: System configuration. Left to right: acoustic wave number projection, source side, niche, plate, niche, receiving side, niche dimensions.

This system consists of four interfaces as shown in Figure 4.2. According to the coordinate definition, the four boundaries will be at $z = \{0, z_p, z_{p+h}, d\}$ where h is the thickness of the plate.

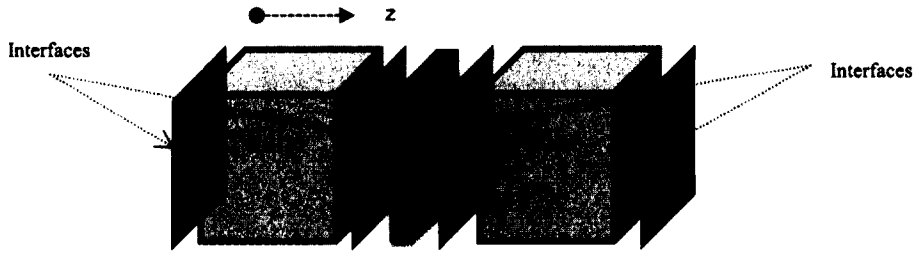

Figure 4.2: System interfaces, left to right: interface between source & niche, niche & plate, plate &niche and niche and receiving.

Boundary conditions, using continuity of pressure and velocity over $S = S_1$, at $z = 0$ are defined as:

$$\begin{cases} \hat{p}_1 = \hat{p}_2 \\ \dfrac{1}{j\omega\rho_0}\dfrac{\partial \hat{p}_r}{\partial z} = \dfrac{1}{j\omega\rho_0}\dfrac{\partial \hat{p}_2}{\partial z} \text{ or } \dfrac{\partial \hat{p}}{\partial z} = \omega^2\rho_0\,\widehat{W}_{a,i}(x,y,z) \end{cases} \quad at\ z = 0 \qquad 4.1$$

The boundary conditions over $S = S_2$ at $z = d$ are:

$$\begin{cases} \hat{p}_3 = \hat{p}_4 \\ \dfrac{1}{j\omega\rho_0}\dfrac{\partial \hat{p}_3}{\partial z} = \dfrac{1}{j\omega\rho_0}\dfrac{\partial \hat{p}_4}{\partial z} \text{ or } \dfrac{\partial \hat{p}}{\partial z} = \omega^2\rho_0\,\widehat{W}_{a,i}(x,y,z\ ) \end{cases} at\ z = d \qquad 4.2$$

where $\widehat{W}_{a,i}(x,y,z)$ is the air particle displacement at point $A(x,y,z)$.

The continuity condition at each side of the plate, z_p, z_{p+h} , are:

$$\widehat{W}(x,y) = \widehat{W}_{a,2}\,(x,y,z_p) \qquad 4.3$$

$$\widehat{W}(x,y) = \widehat{W}_{a,3}\,(x,y,z_{p+h}) \qquad 4.4$$

where, $\widehat{W}\ (x,y,z)$ is plate displacement in z direction. Knowing these conditions will help us to write up the equations in each sub-domain and couple them to each other to have the final matrix of equations.

Total pressure inside medium one ($\hat{p}_1$) is the sum of incident pressure, reflected and radiated pressure from interface:

$$\hat{p}_1 = \hat{p}_{inc} + \hat{p}_R + \hat{p}_r = \hat{p}_b + \hat{p}_r \qquad 4.5$$

Summation of incident pressure and reflected pressure on the surface is defined by blocked pressure, $\hat{p}_b$. In the same methodology of chapter 3 the blocked pressure at $z = 0$ is:

$$\hat{p}_b = 2\widehat{A}_i e^{-jk_0(\sin\theta_i\cos\varphi_i x + \sin\theta_i\sin\varphi_i y)} \qquad 4.6$$

The Rayleigh integral is written for the radiated pressure, $\hat{p}_r$, then boundary conditions, equation 4.1, are used in equation 4.5 at $z = 0$:

$$\hat{p}_1 = \hat{p}_2 = \hat{p}_b + \int_s G(M, M_0) \frac{\partial \hat{p}_2}{\partial z}(M_0) ds \qquad 4.7$$

G, M and M_0 are explained in equations 3.11 to equation 3.13. The homogenous Helmholtz equation and modes of the cavity, the definitions for norm, exciting field, cross modal radiation impedance and acoustic pressure in medium two are, respectively, in the same methodology of chapter 3defined as:

$$\nabla^2 \hat{p}_2(x, y, z) + k_0^2 \, \hat{p}_2(x, y, z) = 0 \qquad 4.8$$

$$\varphi_{pq}(x, y) = \cos\left(\frac{p\pi(x + a)}{2a}\right) \cos\left(\frac{q\pi(y + b)}{2b}\right), \qquad p, q = 0,1,2, \ldots \qquad 4.9$$

$$N_{pq}^2 = \int_s \varphi_{pq}^2(x, y) ds \qquad 4.10$$

$$\hat{F}_{pq} = \int_s \varphi_{pq}(x, y) \, \hat{p}_b ds \qquad 4.11$$

$$\hat{Z}_{uvpq} = \frac{jZ_o K_o}{S} \int_s \int_s \varphi_{uv}(x, y) G(M, M_0) \varphi_{pq}(x_0, y_0) \, ds ds \qquad 4.12$$

$$\hat{p}_2(x, y, z) = \sum_{p=0}^{\infty} \sum_{q=0}^{\infty} \left(\hat{A}_{2,pq} e^{-jK_{2,pq} z} + \hat{B}_{2,pq} e^{jK_{2,pq} z}\right) \varphi_{pq}(x, y) \qquad 4.13$$

So, equation 4.7 at $z = 0$ is rephrased as shown in 4.14:

$$\left(\hat{A}_{2,pq} + \hat{B}_{2,pq}\right) N_{uv}^2 \delta_{uvpq} = \hat{F}_{pq} - \frac{S}{z_0 k_0} \sum_{pq=0}^{\infty} k_{2,pq} \left(\hat{A}_{2,pq} - \hat{B}_{2,pq}\right) \hat{Z}_{uvpq} \qquad 4.14$$

$\hat{A}_{2,uv}, \hat{B}_{2,uv}$ are unknown coefficients. Since the plate is coupled with both fluid domains, and is excited by the pressure difference across the plate, before studying the plate behaviour, the pressure at sub-region three is investigated.

The acoustic pressure in medium three is approximated in terms of propagating and evanescent modes, in the same way of medium two.

$$\hat{p}_3(x,y,z) = \sum_{pq=0}^{\infty} \left(\hat{A}_{3,pq} e^{-jK_{3,pq}\, z} + \hat{B}_{3,pq} e^{jK_{3,pq} z}\right) \varphi_{pq}(x,y) \qquad 4.15$$

Here, $K_{3,pq}$ is as same as $K_{2,pq}$,

$$k_{i,pq} = k_{zpq} = \sqrt{k_0^2 - \left(\frac{p\pi}{2a}\right)^2 - \left(\frac{q\pi}{2b}\right)^2} \quad i = 2,3 \qquad 4.16$$

and $\varphi_{pq}(x,y)$ was mentioned in equation 4.9. $\hat{A}_{3,pq}$ & $\hat{B}_{3,pq}$ are the unknown coefficient vectors and p, q are modes number in x and y direction, respectively. The radiated pressure into medium four, from the Rayleigh integral, is written as:

$$\hat{p}_4 = -\int_s G(M, M_0) \frac{\partial \hat{p}_4}{\partial n}(M_0) ds \quad and \quad \frac{\partial \hat{p}_4}{\partial n} = \frac{\partial \hat{p}_4}{\partial z} \qquad 4.17$$

Using the boundary conditions in equation 4.2 at $= d$, the radiated pressure into medium four is:

$$\hat{p}_4 = \hat{p}_3 = -\int_s G(M, M_0) \frac{\partial \hat{p}_3}{\partial z}(M_0) ds \qquad 4.18$$

The pressure gradient along z, velocity, is written according to homogenous Helmholtz equation:

$$\frac{\partial \hat{p}_3}{\partial z} = -jk_{3,pq}\left(\hat{A}_{3,pq} e^{-jK_{3,pq}\, z} - \hat{B}_{3,pq} e^{jK_{3,pq} z}\right) \varphi_{pq}(x,y) \qquad 4.19$$

Using norm and cross modal radiation impedance definitions, equations 4.10 and 4.12 respectively, equation 4.18 is rephrased as following:

$$\left(\hat{A}_{3,pq}e^{-jK_{3,pq}d}+\hat{B}_{3,pq}e^{jK_{3,pq}d}\right)N_{uv}^{2}\delta_{uvpq}$$
$$=-\frac{S}{z_0k_0}\sum_{pq=0}^{\infty}k_{3,pq}\left(\hat{A}_{3,pq}e^{-jK_{3,pq}d}-\hat{B}_{3,pq}e^{jK_{3,pq}d}\right)\hat{Z}_{uvpq} \quad 4.20$$

So, the radiated pressure into medium four can be calculated by obtaining modal amplitudes $\hat{A}_{3,pq}$ & $\hat{B}_{3,pq}$. Power transmitted will be obtained using pressure and normal velocity on the interface. Before that the plate behavior inside the niche is studied.

For acoustically thin plate, transverse displacement of the plate at position z_p fulfills Kirchhoff's thin plate bending wave equation:

$$\nabla^4\hat{w}(x,y)-k_b^4\hat{w}(x,y)=\frac{1}{\acute{B}}(\hat{p}_2(x,y,z_p)-\hat{p}_3(x,y,z_p)) \quad 4.21$$

where:

$$\nabla^4=\left(\frac{\partial^4}{\partial x^4}+2\frac{\partial^2}{\partial x^2}\frac{\partial^2}{\partial y^2}+\frac{\partial^4}{\partial y^4}\right) \quad 4.22$$

and,

$$k_b=\sqrt[4]{\frac{m\omega^2}{\acute{B}}} \quad 4.23$$

$$\acute{B}=\frac{Eh^3(1+j\eta)}{12(1-\nu^2)} \quad 4.24$$

Here, m is the plate mass per unit area, E is the Young's-modulus, h plate thickness, η is the structural damping, ν is poison ratio and B' is complex bending stiffness. The field variable expansion for transverse displacement of the plate is:

$$\hat{W}_i(x,y)=\sum_{m,n=1}^{\infty}\hat{C}_{mn}\Psi_{mn}(x,y) \quad 4.25$$

The shape function for *simply supported* plate is:

$$\Psi_{mn}(x,y) = \sin\frac{m\pi(x+a)}{2a}\sin\frac{n\pi(y+b)}{2b} \tag{4.26}$$

Where (m,n) denote the number of harmonics along the x and y-coordinate directions. By substituting equations 4.13, 4.15 and 4.25, into the plate equation, 4.21, the following system is obtained;

$$\begin{aligned}\nabla^4 \sum_{mn=1}^{\infty} \hat{C}_{mn}\Psi_{mn}(x,y) - k_b^4 \sum_{mn=1}^{\infty} \hat{C}_{mn}\Psi_{mn}(x,y) \\ = \frac{1}{\hat{B}}\Big(\sum_{pq=0}^{\infty}\big(\hat{A}_{2,pq}e^{-jK_{2,pq}z_p} + \hat{B}_{2,pq}e^{jK_{2,pq}z_p}\big)\varphi_{pq}(x,y) \\ - \sum_{pq=0}^{\infty}\big(\hat{A}_{3,pq}e^{-jK_{3,pq}z_p} + \hat{B}_{3,pq}e^{jK_{3,pq}z_p}\big)\varphi_{pq}(x,y)\end{aligned} \tag{4.27}$$

Multiplying by $\Psi_{rs}(x,y)$ and integrating over S,

$$\begin{aligned}\textstyle\sum_{mn=1}^{\infty}\int_s \Psi_{rs}(x,y)\left(k_x^2+k_y^2\right)^2\hat{C}_{mn}\Psi_{mn}(x,y)ds - \\ k_b^4\textstyle\sum_{mn=1}^{\infty}\int_s \Psi_{rs}(x,y)\,\hat{C}_{mn}\Psi_{mn}(x,y)\,ds = \\ \frac{1}{\hat{B}}\Big(\textstyle\sum_{pq=0}^{\infty}\int_s \Psi_{rs}(x,y)\,\big(\hat{A}_{2,pq}e^{-jK_{2,pq}z_p} + \hat{B}_{2,pq}e^{jK_{2,pq}z_p}\big)\varphi_{pq}(x,y)\,ds - \\ \textstyle\sum_{pq=0}^{\infty}\int_s \Psi_{rs}(x,y)\,\big(\hat{A}_{3,pq}e^{-jK_{3,pq}z_p} + \hat{B}_{3,pq}e^{jK_{3,pq}z_p}\big)\varphi_{pq}(x,y)\,ds\Big)\end{aligned} \tag{4.28}$$

where:

$$K_x = \frac{m\pi x}{2a}, k_y = \frac{n\pi y}{2b} \tag{4.29}$$

$$k_x + k_y = k_b \tag{4.30}$$

Using the plate modes orthogonality:

$$N_{mn}^2 \delta_{mr}\, \delta_{ns} = \int_s \Psi_{mn}(x,y)\, \Psi_{rs}(x,y) ds \tag{4.31}$$

Introducing coupling integral for a rectangular cross section (see Appendix C for the analytical evaluation of this integral):

$$\gamma_{mnuv} = \int_s \Psi_{mn}(x,y) \quad \varphi_{uv}(x,y) ds \tag{4.32}$$

Then:

$$\begin{aligned} \hat{C}_{mn} N_{mn}^2 \left(\left(k_x^2 + k_y^2\right)^2 - k_b^4 \right) & \\ = \frac{1}{\hat{B}} \sum_{pq=0}^{\infty} \left(\hat{A}_{2,pq} e^{-jK_{2,pq} z_p} + \hat{B}_{2,pq} e^{jK_{2,pq} z_p} \right) \gamma_{mnpq} & \\ - \frac{1}{\hat{B}} \sum_{pq=0}^{\infty} \left(\hat{A}_{3,pq} e^{-jK_{3,pq} z_p} + \hat{B}_{3,pq} e^{jK_{3,pq} z_p} \right) \gamma_{mnpq} & \end{aligned} \tag{4.33}$$

The continuity of displacement in z direction between plate and air particles which are over it, at each side of it gives another equation:

$$\begin{aligned} \hat{W}_{a,i}(x,y,z) = \frac{1}{\omega^2 \rho_0} \frac{\partial \hat{p}_i}{\partial z} & \\ = -\frac{j}{\omega^2 \rho_0} \sum_{pq=0}^{\infty} k_{i,pq} \left(\hat{A}_{i,pq} e^{-jK_{i,pq} z} \right. & \\ \left. - \hat{B}_{i,pq} e^{jK_{i,pq} z} \right) \varphi_{pq}(x,y) \quad i = 2,3 & \end{aligned} \tag{4.34}$$

Neglecting the effect of the thickness of the plate, substituting equation 4.254.34 into 4.34:

$$\begin{aligned} \sum_{mn=1}^{\infty} \hat{C}_{mn} \Psi_{mn}(x,y) = -\frac{j}{\omega^2 \rho_0} \sum_{pq=0}^{\infty} k_{2,pq} \left(\hat{A}_{2,pq} e^{-jK_{2,pq} z_p} - \right. & \\ \left. \hat{B}_{2,pq} e^{jK_{2,pq} z_p} \right) \varphi_{pq}(x,y) & \end{aligned} \tag{4.35}$$

$$\sum_{mn=1}^{\infty} \hat{C}_{mn}\Psi_{mn}(x,y) = -\frac{j}{\omega^2\rho_0}\sum_{pq=0}^{\infty} k_{3,pq}\left(\hat{A}_{3,pq}e^{-jK_{3,pq}z_p} - \hat{B}_{3,pq}e^{jK_{3,pq}z_p}\right)\varphi_{pq}(x,y) \quad 4.36$$

By multiplying equations 4.35 and 4.36 by $\varphi_{uv}(x,y)$, integrating over S:

$$\sum_{mn=1}^{\infty}\int_s \varphi_{uv}(x,y)\,\hat{C}_{mn}\Psi_{mn}(x,y)ds =$$
$$-\frac{j}{\omega^2\rho_0}\sum_{pq=0}^{\infty}\int_s \varphi_{uv}(x,y)\; k_{2,pq}\left(\hat{A}_{2,pq}e^{-jK_{2,pq}z_p} - \hat{B}_{2,pq}e^{jK_{2,pq}z_p}\right)\varphi_{pq}(x,y)\; ds \quad 4.37$$

$$\sum_{mn=1}^{\infty}\int_s \varphi_{uv}(x,y)\;\hat{C}_{mn}\Psi_{mn}(x,y)ds =$$
$$-\frac{j}{\omega^2\rho_0}\sum_{pq=0}^{\infty}\int_s \varphi_{uv}(x,y)\; k_{3,pq}\left(\hat{A}_{3,pq}e^{-jK_{3,pq}z_p} - \hat{B}_{3,pq}e^{jK_{3,pq}z_p}\right)\varphi_{pq}(x,y)ds \quad 4.38$$

Using norm (equation 4.10) and coupling (equation 4.32) definitions, we obtain:

$$-\hat{C}_{mn}\gamma_{mnpq} - \frac{j}{\omega^2\rho_0}K_{2,pq}\left(\hat{A}_{2,pq}e^{-jK_{2,pq}z_p} - \hat{B}_{2,pq}e^{jK_{2,pq}z_p}\right)N_{uv}^2\delta_{uvpq} = 0 \quad 4.39$$

$$-\hat{C}_{mn}\gamma_{mnpq} - \frac{j}{\omega^2\rho_0}K_{3,pq}\left(A_{3,pq}e^{-jK_{3,pq}z_p} - B_{3,pq}e^{jK_{3,pq}z_p}\right)N_{uv}^2\delta_{uvpq} = 0 \quad 4.40$$

Equations 4.14, 4.39, 4.33, 4.40, and 4.20 are written in matrix format, respectively.

$$\begin{bmatrix} \xi_1 & \xi_2 & 0 & 0 & 0 \\ \xi_3 & \xi_4 & \xi_5 & 0 & 0 \\ \xi_6 & \xi_7 & \xi_8 & \xi_9 & \xi_{10} \\ 0 & 0 & \xi_{11} & \xi_{12} & \xi_{13} \\ 0 & 0 & 0 & \xi_{14} & \xi_{15} \end{bmatrix}_{h\times h} \begin{Bmatrix} \hat{A}_{2,pq} \\ \hat{B}_{2,pq} \\ \hat{C}_{mn} \\ \hat{A}_{3,pq} \\ \hat{B}_{3,pq} \end{Bmatrix}_{h\times 1} = \begin{Bmatrix} \hat{F}_{pq} \\ 0 \\ 0 \\ 0 \\ 0 \end{Bmatrix}_{h\times 1} \quad 4.41$$

where, ξ_i are sub matrices and their rank is related to the number of kept modes. The rank of general matrix, which is complex and non-symmetric, and sub matrices are defined in the following:

$$h = 4 \times (p_{max} + 1) \times (q_{max} + 1) + (m_{max} \times n_{max}) \quad 4.42$$

where $\{p_{max}, q_{max}\}$ and $\{m_{max}, n_{max}\}$ are the maximum number of kept modes in $\{x, y\}$ direction for niche and plate respectively:

$$\xi_{1,uvpq} = N_{uv}^2 \delta_{uvpq} + \frac{S}{Z_0 K_0} \sum_{pq=0}^{\infty} k_{2,pq} \hat{Z}_{uvpq} \quad 4.43$$

$$\xi_{2,uvpq} = N_{uv}^2 \delta_{uvpq} - \frac{S}{Z_0 K_0} \sum_{pq=0}^{\infty} k_{2,pq} \hat{Z}_{uvpq} \quad 4.44$$

$$\xi_{3,uvpq} = -\frac{j}{\omega^2 \rho_0} k_{2,pq} N_{uv}^2 \delta_{uvpq} e^{-jK_{2,pq} z_p} \quad 4.45$$

$$\xi_{4,uvpq} = \frac{j}{\omega^2 \rho_0} k_{2,pq} N_{uv}^2 \delta_{uvpq} e^{jK_{2,pq} z_p} \quad 4.46$$

$$\xi_{5,uvmn} = -\gamma_{uvmn} \quad 4.47$$

$$\xi_{6,mnpq} = -\frac{1}{\acute{B}} \sum_{pq=0}^{\infty} \gamma_{mnpq} e^{-jK_{2,pq} z_p} \quad 4.48$$

$$\xi_{7,mnpq} = -\frac{1}{\acute{B}} \sum_{pq=0}^{\infty} \gamma_{mnpq} e^{jK_{2,pq} z_p} \quad 4.49$$

$$\xi_{8,mnrs} = \left(\left(k_x^2 + k_y^2\right)^2 - K_b^4 \right) N_{rs}^2 \delta_{mnrs} \quad 4.50$$

$$\xi_{9,mnpq} = \frac{1}{\acute{B}} \sum_{pq=0}^{\infty} \gamma_{mnpq} e^{-jK_{3,pq} z_p} \quad 4.51$$

$$\xi_{10,mnpq} = \frac{1}{\acute{B}} \sum_{pq=0}^{\infty} \gamma_{mnpq} e^{jK_{3,pq} z_p} \quad 4.52$$

$$\xi_{11,pqmn} = -\gamma_{pqmn} \quad 4.53$$

$$\xi_{12,uvpq} = -\frac{j}{\omega^2 \rho_0} k_{3,pq} N_{uv}^2 \delta_{uvpq} e^{-jK_{3,pq} z_p} \quad 4.54$$

$$\xi_{13,uvpq} = \frac{j}{\omega^2 \rho_0} k_{3,pq} N_{uv}^2 \delta_{uvpq} e^{jK_{3,pq} z_p} \quad 4.55$$

$$\xi_{14,uvpq} = e^{-jK_{3,pq} d} N_{uv}^2 \delta_{uvpq} + \frac{S}{Z_0 K_0} \sum_{pq=0}^{\infty} k_{3,pq} \hat{Z}_{uvpq} e^{-jK_{3,pq} d} \quad 4.56$$

$$\xi_{15,uvpq} = e^{jK_{3,pq} d} N_{uv}^2 \delta_{uvpq} - \frac{S}{Z_0 K_0} \sum_{pq=0}^{\infty} k_{3,pq} \hat{Z}_{uvpq} e^{jK_{3,pq} d} \quad 4.57$$

4.2.1 Calculation of vibro-acoustic indicators

The equation 4.41 is implemented in a FORTRAN code and solved for a given incident oblique plane wave and diffuse acoustic field, using the linear algebra package "LAPACK".

As mentioned before, the objective of this study is to investigate the effect of niche parameters on STL. By definition, the transmitted power is given by:

$$\Pi_t(\theta_i, \varphi_i) = \frac{1}{2} Re \left[\int_s p u_n^* ds \right] \quad 4.58$$

where u_n^* is the complex conjugate normal velocity at $z = d$. The pressure in medium two and three can be calculated by substituting the coefficients $\hat{A}_{2,pq}, \hat{B}_{2,pq}, \hat{A}_{3,pq}, \hat{B}_{3,pq}$ into equations 4.13 and 4.15 . As mentioned before, the incident and transmitted power are necessary for calculating sound transmission loss. So, the transmitted acoustic power for one oblique incident plane wave is calculated as following:

$$\Pi_t(\theta_i, \varphi_i) = \tfrac{1}{2} Re \left[\int_s \hat{p}_4 \hat{u}_{4,n}^* ds \right] =$$
$$\tfrac{1}{2} Re \left[\frac{j}{\rho_0 \omega} \int_s \sum_{pq=0}^{\infty} \left(\hat{A}_{3,pq} e^{-jK_{3,pq} d} + \right. \right. \quad 4.59$$
$$\left. \left. \hat{B}_{3,pq} e^{jK_{3,pq} d} \right) \varphi_{pq}(x,y) \sum_{uv=0}^{\infty} K_{3,uv}^* \left(-\hat{A}_{3,uv} e^{-jK_{3,uv} d} + \right. \right.$$

$$\hat{B}_{3,uv}e^{jK_{3,uv}d})^{*}\varphi_{uv}(x,y)\,ds\Big] = \frac{1}{2}Re\left[\frac{-1}{\rho\omega}\,\hat{D}_{pq}N_{pq}^{2}\,K^{*}_{3,pq}\hat{E}^{*}_{pq}\right]$$

$$\hat{D}_{pq} = \hat{A}_{3,pq}e^{-jK_{3,pq}\,d} + \hat{B}_{3,pq}e^{jK_{3,pq}d} \qquad 4.60$$

$$\hat{E}_{pq} = -\hat{A}_{3,pq}e^{-jK_{3,pq}\,d} + \hat{B}_{3,pq}e^{jK_{3,pq}d} \qquad 4.61$$

The incident power is given by:

$$\Pi_{inc}(\theta_i,\varphi_i) = \frac{|A_i|^2\cos\theta_i S}{2\rho_0 c_0} \qquad 4.62$$

Then, by employing the oblique incidence transmission coefficient, τ, the transmission loss will be calculated;

$$\tau(\theta_i,\varphi_i) = \frac{\Pi_t\,(\theta_i,\varphi_i)}{\Pi_{inc}\,(\theta_i,\varphi_i)} \qquad 4.63$$

$$STL = -10\log\tau \qquad 4.64$$

4.2.2 Transmitted power for diffuse acoustic field

Since there are more than one plane wave in diffuse acoustic field, the unknown coefficient vectors and exciting force sub-matrices are changed as following:

$$\begin{bmatrix} \xi_1 & \xi_2 & 0 & 0 & 0 \\ \xi_3 & \xi_4 & \xi_5 & 0 & 0 \\ \xi_6 & \xi_7 & \xi_8 & \xi_9 & \xi_{10} \\ 0 & 0 & \xi_{11} & \xi_{12} & \xi_{13} \\ 0 & 0 & 0 & \xi_{14} & \xi_{15} \end{bmatrix}_{h\times h} \begin{Bmatrix} \hat{A}_{2,pq} & \cdots & \hat{A}'_{2,pq} \\ \hat{B}_{2,pq} & \cdots & \hat{B}'_{2,pq} \\ \hat{C}_{mn} & \cdots & \hat{C}'_{mn} \\ \hat{A}_{3,pq} & \cdots & \hat{A}'_{3,pq} \\ \hat{B}_{3,pq} & \cdots & \hat{B}'_{3,pq} \end{Bmatrix}_{h\times k} \qquad 4.65$$

$$= \begin{Bmatrix} \hat{F}_{pq} & \cdots & \hat{F}'_{pq} \\ 0 & \cdots & 0 \\ 0 & \cdots & 0 \\ 0 & \cdots & 0 \\ 0 & \cdots & 0 \end{Bmatrix}_{h\times k}$$

where h is defined in equation 4.42 and k is:

$$k = number\ of\ Gauss\ points\ across\ \theta \times number\ of\ Gauss\ points\ across\ \varphi \quad 4.66$$

Here, $\hat{A}'_{2,pq}$, $\hat{B}'_{2,pq}$, $\hat{C}'_{mn}$, $\hat{A}'_{3,pq}$ and $\hat{B}'_{3,pq}$ are unknowns associated to i^{th} plane wave and $\hat{F}'_{pq}$ is the exciting force associated from that plane wave. Plane wave Transmission coefficient is calculated as following:

$$\tau_{diff} = \frac{\int_0^{2\pi}\int_0^{\theta_{lim}} \tau(\theta_i, \varphi_i) \sin\theta_i \cos\theta_i \, d\theta d\varphi}{\pi \sin^2 \theta_{\lim}} \quad 4.67$$

where $\tau(\theta_i, \varphi_i)$ is the transmission coefficient for each plane wave and

$$\theta_{lim} = 78° \left(\frac{\pi}{180}\right) \quad 4.68$$

The transmission loss is calculated as shown in equation 4.64. Radiation efficiency can be calculated as:

$$\sigma_{rad} = \frac{\Pi_t}{\rho c_0 S < \overline{u_n^2} >} \quad 4.69$$

Here $\overline{u^2}$, is the spatial average of mean square velocity of the plate and is calculated by substituting boundary conditions 4.3 and 4.4 into 4.1 and 4.2. Transmitted power can be calculated by using equation 4.59.(since the fluid damping is neglected, the radiated power at the end of the niche is the same of the radiated power over the plate).

4.3 Numerical model

In this section several examples are presented to validate the approach. First of all, the convergence of acoustic indicators, sound transmission loss, radiation efficiency and power transmitted have been studied by looking at the number of modes which are taken into account by increasing the truncation frequencies, for both plate and niche. In the second step, the approach is validated by comparing the results obtained by FEM-BEM method.

4.3.1 Problem definition

The dimensions of the niche and plate and the place of plate inside niche for model are given in Table 4.1. This system can be filled up by four fluids, in spite of this, here, all the fluids have the same characters as air, the density of the fluid *(ρ_0)*, speed of sound inside air *(C_0)* are shown in Table 4.2. And finally, the plate mechanical characteristics, Young's modulus *(E)*, Poisson's ratio *(v)*, damping ratio *(η)* and density *(ρ_s)*, are detailed in Table 4.3.

Table 4.1: The dimensions of niche, plate and plate position inside the niche:

$a\,(m)$	$b\,(m)$	$(d)\,(m)$	$Z_p\,(m)$	$h\,(m)$
0.3	0.2	0.1	0.05	0.008

Table 4.2: Fluid characteristics:

$\rho_0 = \rho_1 = \rho_2 = \rho_3 = \rho_4\ (kg/m^3)$	$C_0 = C_1 = C_2 = C_3 = C_4\ (m/s)$
1.213	342.2

Table 4.3: Plate mechanical characteristics

$E(Gpa)$	v	η	$\rho_s(\mathrm{kg/m^3})$
69	0.33	0.03	2742

4.3.2 Convergence of the approach

Convergence is highly dependent on the number of structural and acoustical modes which are kept into account according to the truncation frequency in the proposed method. This frequency can be the same or larger than maximum frequency. In order to determine the

truncation frequency, convergence of acoustic indicators, such as: transmission loss, radiation efficiency and power transmitted are investigated for two kind of excitation, first plane wave and then diffuse acoustic field. Before that excitation parameters for both plane wave and diffuse field are detailed in Table 4.4.

Table 4.4: Excitation characteristics for niche-plate system.

Pressure amp.	Frequency	Plane wave		Diffuse acoustic field		
A_i (pa)	f_{min}- f_{max}(Hz)	Θ	φ	Number of Gauss points in Θ	Number of Gauss points in φ	Θ_{lim}
1	10- 2000	45°	60°	20	20	78°

The ratio of truncation frequency to maximum interested frequency is defined as non-dimensional number, α:

$$\alpha_a = \frac{f_{truncation,acoustical}}{f_{max}} \quad 4.70$$

$$\alpha_s = \frac{f_{truncation,structural}}{f_{max}} \quad 4.71$$

The truncation frequency can be different for structural part than acoustical part. So, two numbers, for structural and acoustical parts, are defined as (α_s, α_a) respectively. In the first step, modes of the plate and niche are kept up to two times of the maximum frequency of interest, $(\alpha_s, \alpha_a) = (2,2)$ and are considered as reference. A laptop which has 2.4 GHz corei3 CPU and 4 GB ram is used for the calculations. In the next step, modes are kept up to f_{max} *and* $1.5f_{max}$ for both plate and niche. As shown in Figure 4.3, keeping acoustical modes up to the maximum frequency, $(\alpha_s, \alpha_a) = (2,1)$ is not good enough to capture the physics of the problem; discrepancy is more than 1 (dB) at high frequency range, while keeping plate modes up to the maximum frequency suffices to have a good convergence, $(\alpha_s, \alpha_a) = (1,2)$. So, the number of acoustical modes has considerable effect on the convergence. Increasing the number of modes and comparing the results with reference system reveals that keeping the truncation frequency the same as f_{max} for the plate and increasing the truncation frequency of

the niche up to $(\alpha_s, \alpha_a) = (1, 1.3)$ and $(\alpha_s, \alpha_a) = (2, 1.5)$, is enough to capture the physics of the problem. In the following figures, Δ, means that all the acoustic indicators are compared to the $(\alpha_s, \alpha_a) = (2, 2)$.

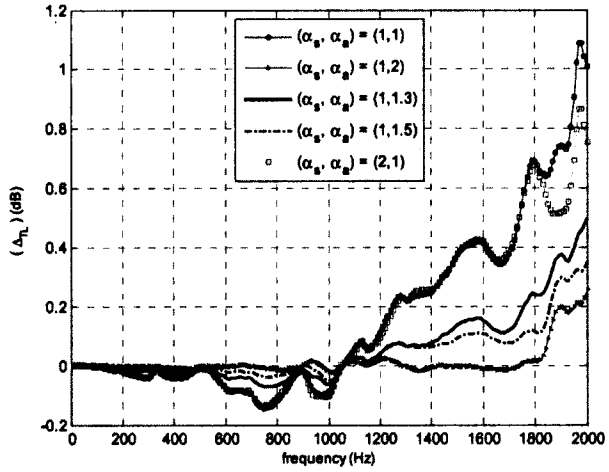

Figure 4.3: Effect of number of modes on convergence of STL, plane wave acoustic field.

Two other acoustic indicators, Radiation efficiency and Power transmitted, are shown in Figure 4.4. As shown in these figures, considering acoustic modes up to 1.3 times of maximum frequency meets the requirements of capturing the physics of the problem for acoustical plane wave excitation.

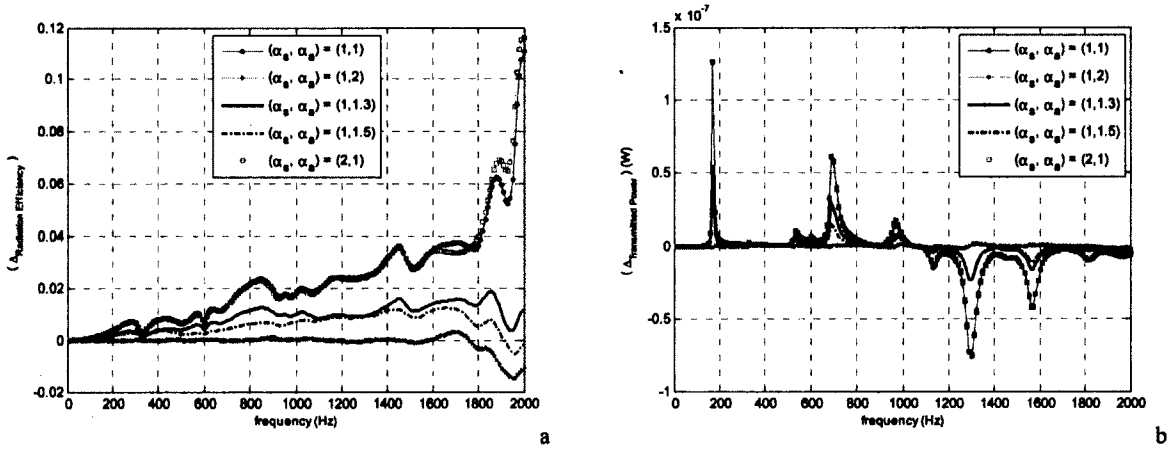

Figure 4.4: The effect of number of modes on convergence of a) σ_R, b) Π_t , plane wave acoustic field.

Since the parameter study of the system in addition to plane wave field will be done under diffuse acoustic field excitation, the convergence of the system at two truncation frequencies for diffuse acoustic field, $(\alpha_s, \alpha_a) = (1, 1.3)$ and $(\alpha_s, \alpha_a) = (1, 1.5)$, are investigated. The effect of truncation frequency on transmission loss, radiation efficiency and power transmitted are shown in Figure 4.5, Figure 4.6. So, considering these results and because of the computation cost and memory issue (calculation time reduces from 1000 seconds when $(\alpha_s, \alpha_a) = (1, 1.5)$ to 500 seconds when $(\alpha_s, \alpha_a) = (1, 1.3)$), the truncation frequency will be considered as $1.3f_{max}$ during this study. It should be note that this is fine as long as damping is low in both systems (niche and plate). For the maximum frequency of $4000\,Hz$, 400 acoustic modes and 324 structural modes are taken into account.

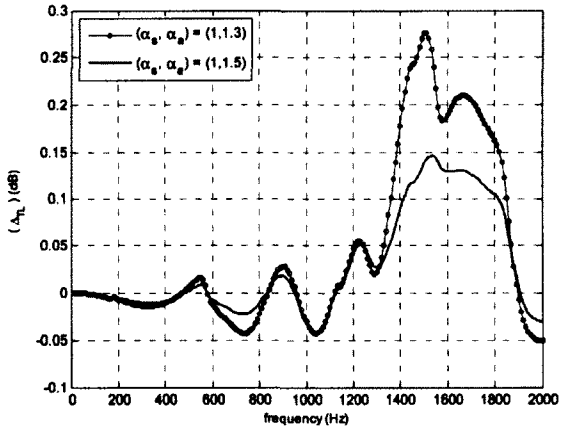

Figure 4.5: The effect of number of modes on convergence of STL, Diffuse acoustic field.

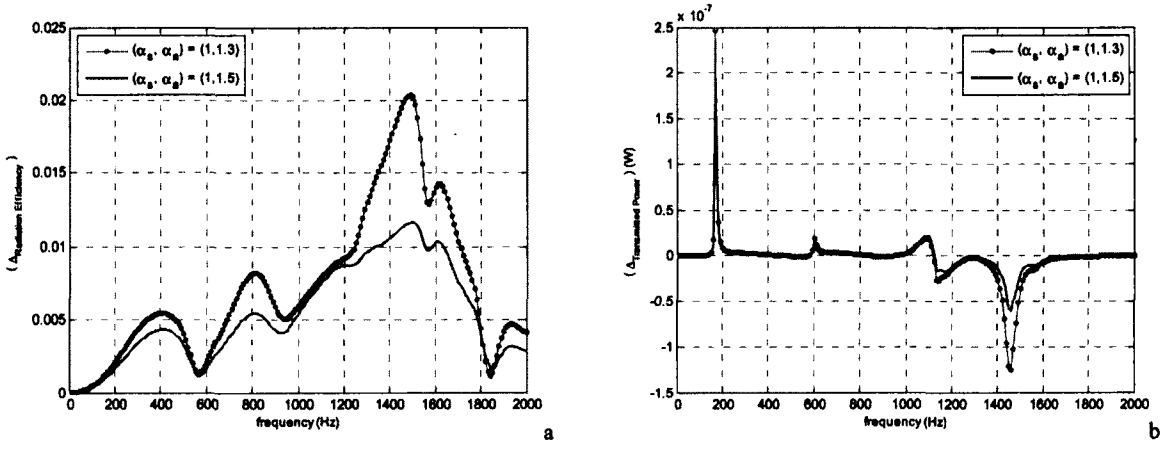

Figure 4.6: Effect of number modes on convergence of a) σ_R, b) Π_t, Diffuse acoustic field.

4.4 Model validation

The results of proposed method are validated by comparison with FEM-BEM in NOVAFEM. The niche and plate system are modeled as shown in Figure 4.2. "QUAD" plate elements are used for the admittance matrix and fluid-structure coupling elements, the niche volume is discretized using acoustic brick (Hexa8) elements and the plate is discretized using Hexa 8 solid elements (plate elements are not used since acoustic pressure is non-continuous through the plate). The physical properties of the fluid and plate are given in Table 4.1 and Table 4.2. The dimensions of the system (x, y, d), plate position inside the niche, z_p, and number of the elements are given in Table 4.5. The dimensions of the plate and niche in $x - y$ directions are the same. So, the number of elements along x and y are the same for niche and plate. Since the convergence is slow, Figure 4.7, 12 elements per wave length, λ_a, are used to mesh the niche (acoustic domain).

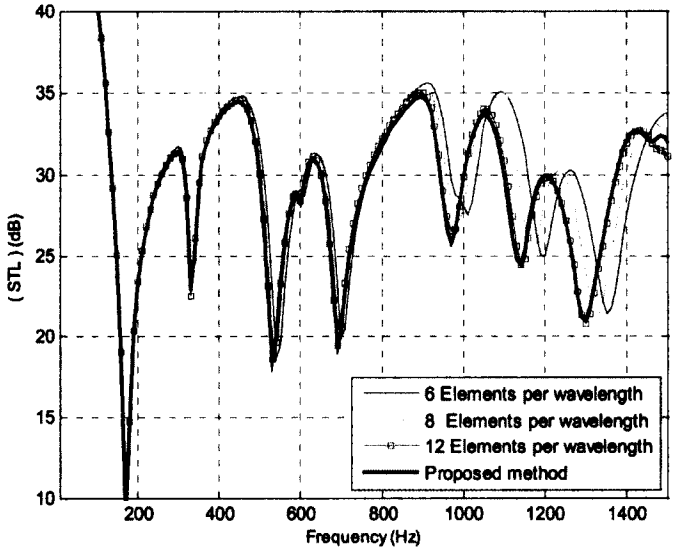

Figure 4.7: Convergence of the model in NOVAFEM for 6, 8 and 12 elments per wavelength.

$$\lambda_a = \frac{c_0}{f_{max}} \approx 0.18\,(m) \qquad 4.72$$

Table 4.5: Dimension and number of elements for the niche and plate in NOVAFEM

	$2a\,(m)$	$2b(m)$	$d(m)$	$h(m)$	$z_p(m)$
Dimension	0.6	0.4	0.08	0.008	0.04
Elements	40	30	8	2	

The oblique acoustic plane wave excitation, Table 4.4, is considered here, and the transmission loss of the system obtained by proposed method and NOVAFEM are shown in Figure 4.8 and excellent agreement is observed.

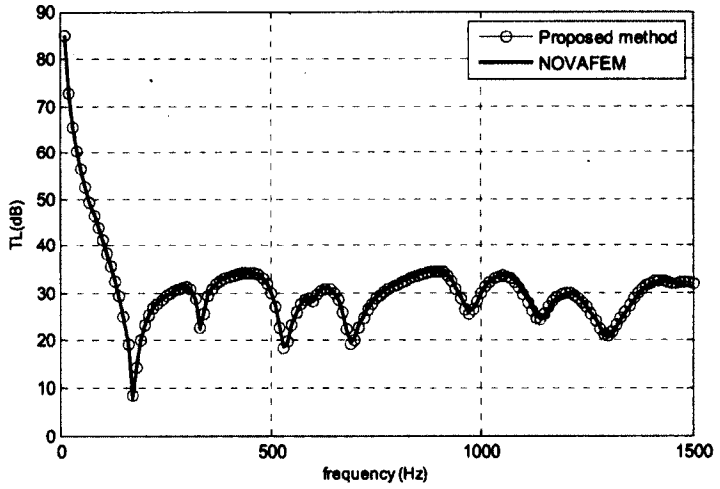

Figure 4.8: Validation of proposed method; Transmission loss of niche-pate system under oblique plane wave excitation.

Proposed method is next validated in two other conditions; first, previous example under diffuse acoustic field excitation, Figure 4.9.a. Second, plate is flushed mounted in front side of the niche, Figure 4.9.b. It should be noted that it takes 55800 seconds to calculate the FEM-BEM model on super computer of the Sherbrooke University while this time reduces to 330 seconds through proposed method using the corei3 laptop. As shown in these figures our model being validated the next section investigates the effect of niche parameters on STL.

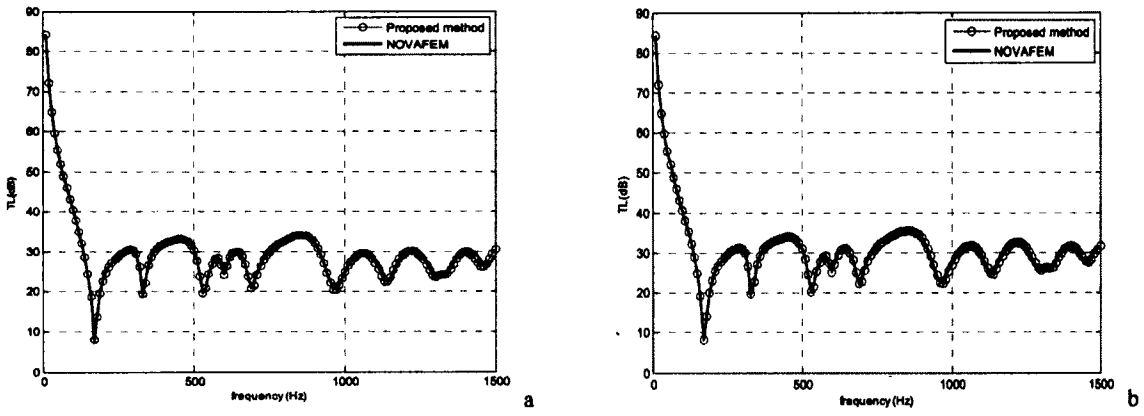

Figure 4.9: Validation of proposed method, diffuse acoustic field excitation. a) Plate placed at the center of the niche. b) Plate is flushed mounted at the front side of their niche.

4.5 Parameters study

As mentioned in section 2.1, plate positions inside the niche and niche depth have more effects on STL. The effect of these parameters on sound transmission loss of the baffled plate is studied in this section. The STL of the same plate placed in rigid baffle separating the two semi-infinite fluids is considered as a baseline for the comparison. So, the niche effect is measured by the difference between niche-STL and reference plate–STL is defined as niche effect (Insertion Loss):

$$IL = STL_{niche} - STL_{ref} \qquad 4.73$$

Niche can be placed in front or back side or both sides of the plate. So, it affects excitation field, radiation efficiency or both of them, respectively. The case, in which plate is inside the niche, falls into two sub-systems; in the first one, effect of niche on excitation field is considered. To this end, plate is placed at the end of the niche, or in the other words, it is flushed mounted in the back side of the niche. In this system, niche affects the excitation field while the radiation part of the plate remains as for the baffled plate. In the second sub-system, plate is flushed mounted in the front side of the niche. In this position, the excitation field is the same as for the baffled plate, while plate is radiating into the niche. Consequently, the

effect of niche on excitation field in the former, and on radiation field in the latter position is investigated separately.

4.5.1 Effect of niche on excitation

Excitation field is affected by niche existence. In the other word, the excitation field over the plate is different than baffled plate because plate is excited through niche. Niche and plate in this situation are shown in Figure 4.10.

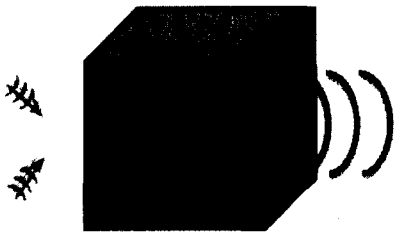

Figure 4.10: Plate placed at the back side of the niche.
Niche affects the excitation field

In order to investigate the niche effect, the results are compared with this reference system; the oblique plane wave is considered as mentioned in Table 4.4. The effect of adding niche on STL is shown in Figure 4.11 and Figure 4.12. As shown in these figures, niche decreases the STL up to 6 dB when frequency range is below critical frequency of the baffled plate. Considering the equation 4.63, transmission loss depends on ratio of incident power and transmitted power through the system. The incident power is the same in both systems; so, the effect of niche on transmitted power is the reason of discrepancy between STL of these two systems.

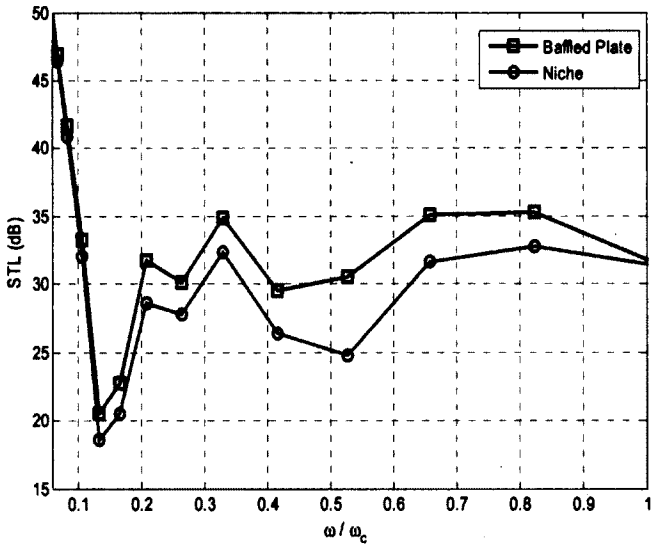

Figure 4.11: STL average in 1/3 octave band, plate is placed at the back side of the niche.

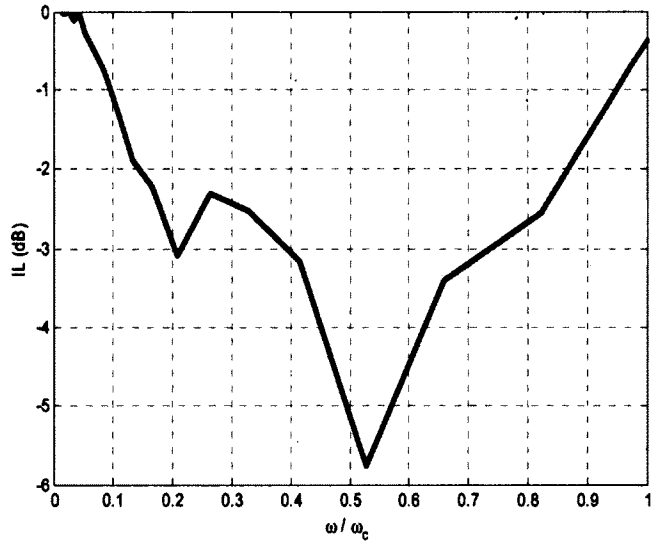

Figure 4.12: Niche effect average in 1/3 octave band, plate is placed at back side of the niche.

The power transmitted to the receiving side is shown in Figure 4.13 . As shown in this figure, niche increase power transmitted in the same frequencies in which the STL of niche is less than STL of the reference system.

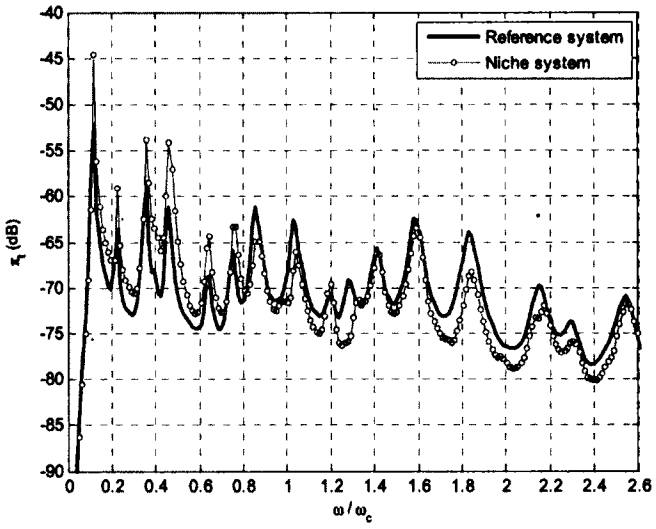

Figure 4.13: Transmitted power through the plate.

Considering the radiation efficiency formula, the transmitted power through the panel depends on two factors: panel vibration and radiation efficiency.

As mentioned in equation 4.21, the vibration field are excited by the pressure difference across the plate; Effect of niche on radiation efficiency is depicted in Figure 4.14. Niche doesn't have considerable effect on radiation efficiency of the plate for this position of the plate (the radiation side of the plate is the same as radiation side of the baffled plate); while, the power transmitted varies because of the niche. Consequently the quadratic velocity of the plate should have the same behaviour as transmitted power, Figure 4.15. The conclusion of these results is that, niche affects the vibration field by increasing the pressure difference across the plate. So, the blocked pressure, as exciting pressure, inside the niche increases.

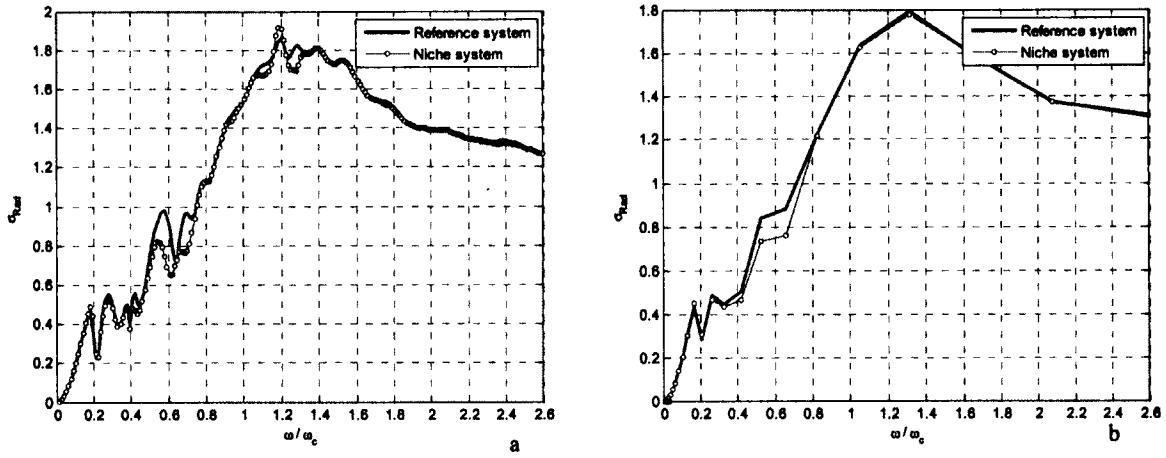

Figure 4.14: Radiation efficiency, plate is placed at the back side of the niche; a) Narrow band, b) 1/3 Octave band.

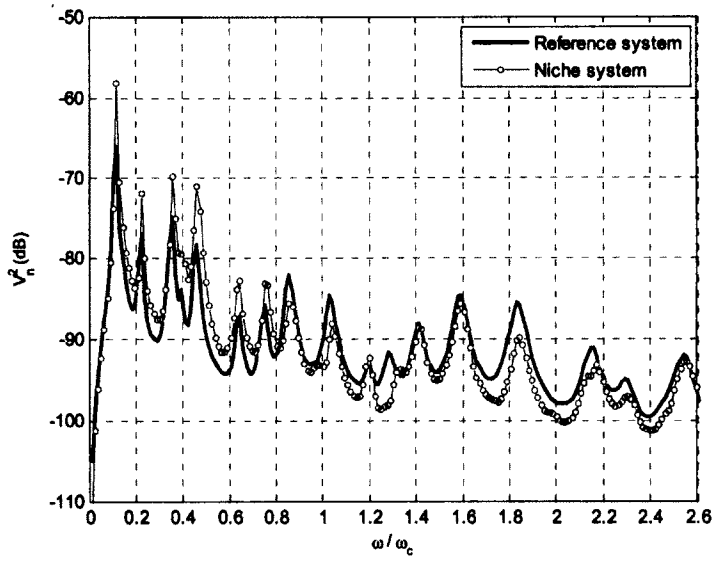

Figure 4.15: Mean square velocity, plate is placed at the back side of the niche.

Excitation field applying on the plate is associated with the pressure over the plate. So, increase in velocity means increase in pressure over the plate. Pressure on the plate which is placed inside niche, $\hat{p}_2$, consists of blocked and radiated pressure.

In order to see the influence of radiated pressure of the baffled plate, the ratio of quadratic total pressure over the baffled plate (no niche), to the theoretical quadratic blocked pressure of the baffled plate in theory is shown in Figure 4.16. As shown here, except of the first mode

where the radiation efficiency has the maxima, the effect of radiated pressure is negligible over the frequency range.

$$20\log\left(\frac{\hat{p}_{total\ over\ baffled\ plate}}{\hat{p}_{b_{Baffled\ plate\ in\ theory}}}\right) = \varepsilon \qquad 4.74$$

$$for\ \varepsilon \to 0,\quad 1 + \frac{\hat{p}_r}{\hat{p}_{b_{plate,theory}}} \approx 1 \to \hat{p}_r \approx 0 \qquad 4.75$$

In this model the total pressure applying on the plate inside the niche, $\hat{p}_2$ is calculated. Since, this difference in total pressure across the plate controls the response, we will use the total pressure to investigate the difference between the baffled case and the niche configurations (in both configurations the fluid loading is included in the excitation term). The ratio of the total quadratic pressure affected by the niche to the total pressure of the baffled plate is shown in Figure 4.17.

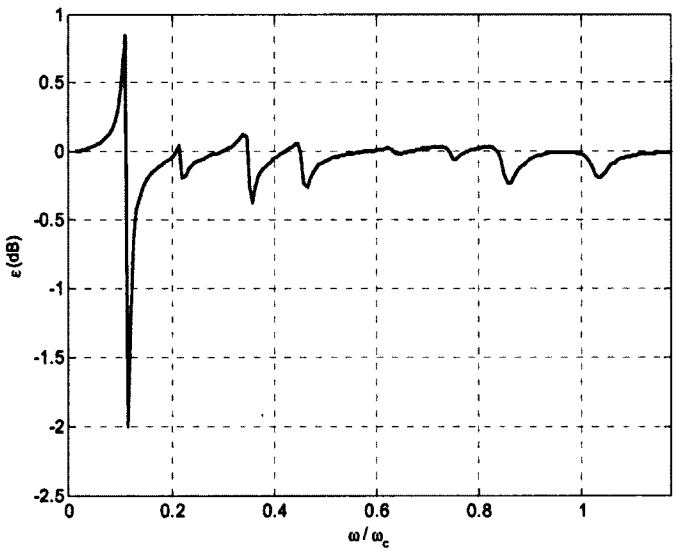

Figure 4.16: Effect of total pressure over the blocked pressure when d/a=1/3.

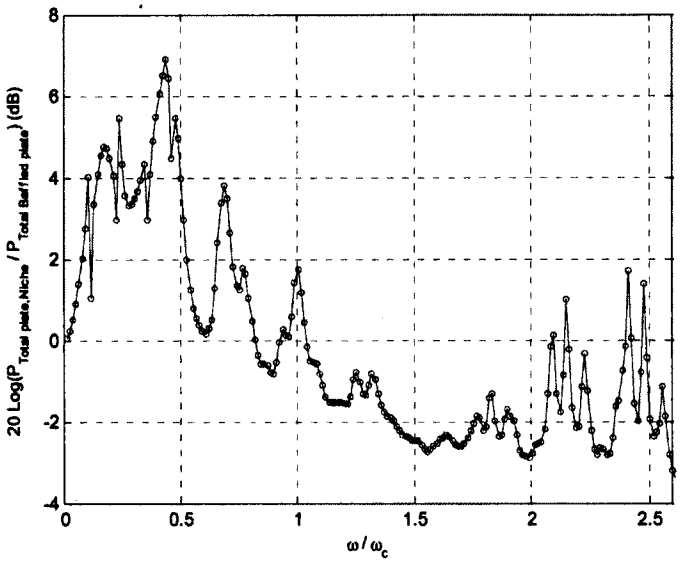

Figure 4.17: Effect of niche on total pressure.

As shown here, the quadratic parietal pressure increases up to 7 (dB) before critical frequency, then it reduces in comparison with the baffled plate. Hence, the effect of niche is increasing the pressure. This increase is more considerable at corners and edges, where finite plate has maximum radiation. Figure 4.18 shows the pressure for three points, center, edge and corner, on the plate and inside the niche and the space averaged integral of the pressure over the surface of the plate.

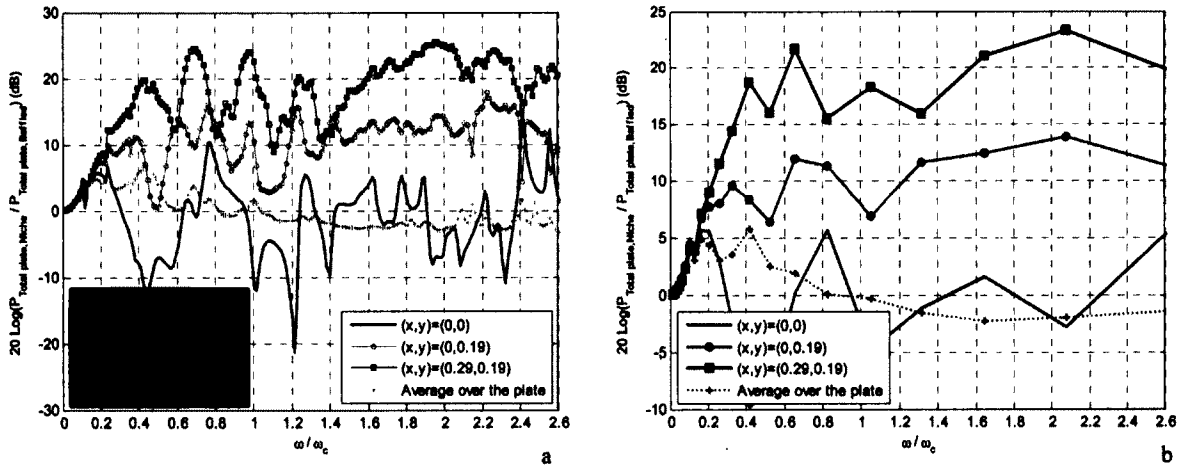

Figure 4.18: Pressure inside the niche, at three points: center, edge and corner; a) Narrow band, b) 1/3 Octave band.

4.5.2 Effect of niche-depth on excitation

Effect of niche on excitation was studied in previous section. Here, effect of niche-depth on excitation is investigated. Before study the effect of niche depth on STL, the acoustic wave length and its associated frequency, in $x-y$ plane and z direction, is calculated. The wave number and wavelength over the $x-y$ and z can be calculated as:

$$|k_{xy}| = \sqrt{k_x^2 + k_y^2} = k_o \sin\theta_i \qquad 4.76$$

$$\lambda_{xy} = \frac{2\pi}{|k_{xy}|} = \frac{\lambda_o}{\sin\theta_i} \qquad 4.77$$

$$\lambda_z = \frac{2\pi}{|k_z|} = \frac{\lambda_o}{cos\,\theta_i} \qquad 4.78$$

Here, k_{xy}, k_z and λ_{xy}, $\lambda_z$are the acoustic wave number and acoustic wavelength on $x-y$ plane and z direction, respectively. Behaviour of system is studied when the acoustic wavelength is a ratio of geometric dimensions of the system. These ratios are shown in Table4.6.

Table4.6: Corresponding frequency in which λ_a is a multiplication of niche dimensions

	λ_{xy}						λ_z & $\frac{d}{a}=\frac{1}{3}$		
	$\frac{\lambda_{xy}}{a}=2$	$\frac{\lambda_{xy}}{b}=2$	$\frac{\lambda_{xy}}{a}=1$	$\frac{\lambda_{xy}}{b}=1$	$\frac{\lambda_{xy}}{a}=0.25$	$\frac{\lambda_{xy}}{b}=0.25$	$\frac{\lambda_z}{d}=2$	$\frac{\lambda_z}{d}=1.5$	$\frac{\lambda_z}{d}=1$
ω/ω_c	0.5	0.8	1	1.6	2.12	3.2	3.2	2.12	1.6

The effect of niche-depth on total pressure over the plate while its length varies from $\frac{d}{a}=\frac{1}{6}$ to $\frac{d}{a}=\frac{1}{2}$ is shown in Figure 4.19. As shown here, the total pressure over plate increases with the depth of the niche. This effect is more considerable at low frequencies. Niche shows different behaviour when $\frac{\omega}{\omega_c}=0.5$, at this frequency λ_{xy} is equal to maximum plate dimension, 2a. From this point ahead, because of reflection from interior walls, the acoustic field inside the niche changes to stationary field (modal behaviour). This change will cause reduction in pressure. For the longer niche, the effect of increasing pressure over the plate is more considerable but the change in acoustic field inside the niche happens at lower frequencies. Subsequently, the pressure increases where niche depth is well smaller than acoustic wavelength in z direction. Figure 4.20 and Figure 4.21, show the effect of niche-depth on STL. Niche increases the resonant transmission, so, STL decreases at eigen-frequencies of the system (which are close to the eigen-frequencies of the plate). For the small depth, before critical frequency, niche STL remains smaller than reference plate STL, after that niche effect diminishes. For $\frac{d}{a}=\frac{1}{6}$, the STL is decreased up to 4 dB before critical frequency, while for double length, STL decreases up to7dB, and 8 dB when depth-ratio is $\frac{d}{a}=\frac{1}{2}$.

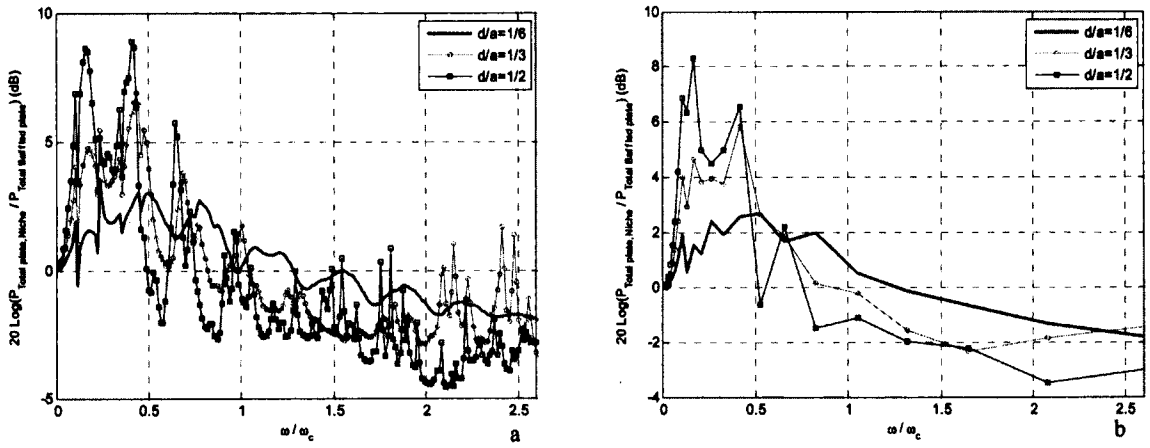

Figure 4.19: Effect of niche depth on total pressure; a) Narrow band, b) 1/3 Octave band.

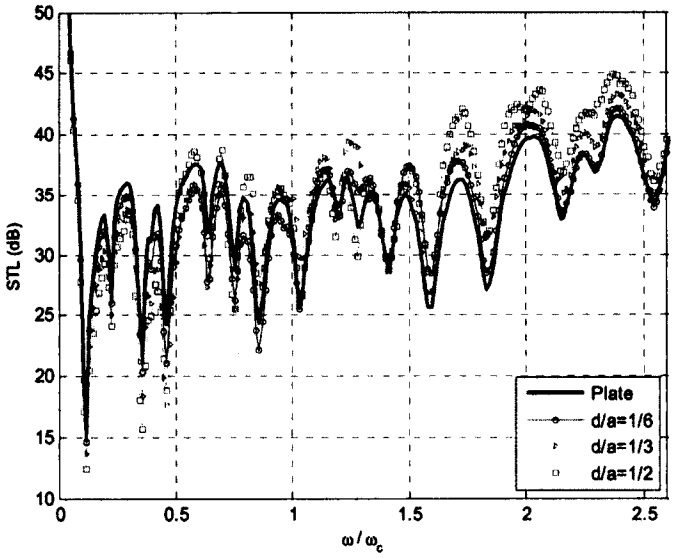

Figure 4.20: Effect of niche-depth on STL.

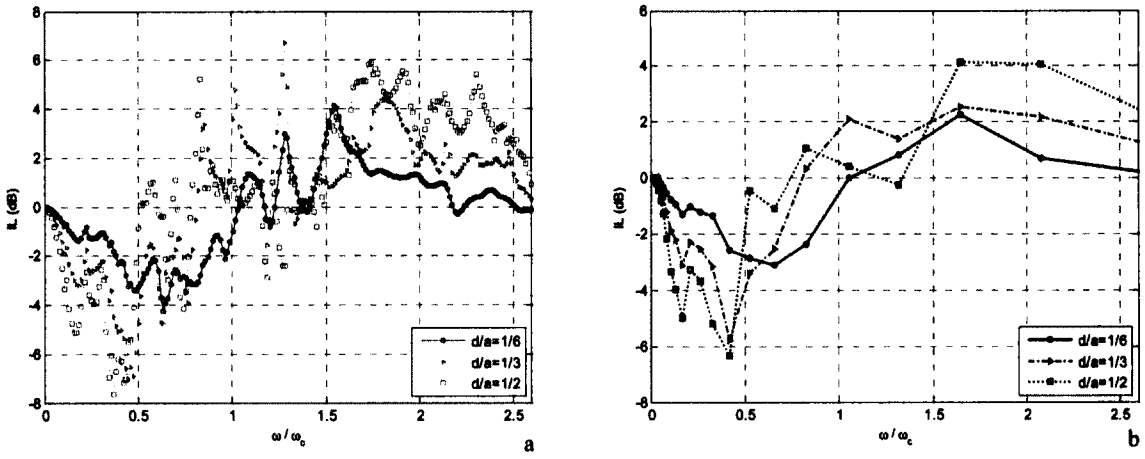

Figure 4.21: Niche effect for three different lengths; a) Narrow band, b) 1/3 Octave band.

In the second system, $\frac{d}{a} = \frac{1}{3}$, when $\frac{\omega}{\omega_c} = 1.6$, acoustic wavelength in z direction is equal to the niche depth. In addition, λ_{xy} becomes equal to the half of smaller dimension of the niche (b). In this case the acoustic wavelength is less than $\frac{1}{2}$ dimension of the niche; therefore the only propagating mode isn't the plane wave mode and the reflection from interior walls leads to fully modal filed inside the niche.

According to what mentioned here, the effect of niche is increasing the pressure inside the niche, this causes an increase in vibration field of the plate and the transmitted power increases while the radiation efficiency remains almost the same.

4.5.3 Effect of niche on radiation

In this section the effect of niche on radiation of the plate is studied. To this end, plate is placed in front side of the niche, Figure 4.22. As shown in this figure, plate first radiates inside the niche and then system radiates into the SIF.

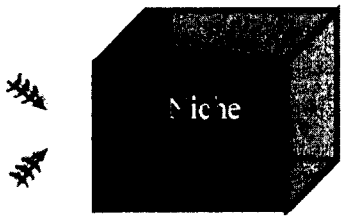

Figure 4.22: Effect of niche on radiation field.

In this model, in the same way of section 4.5.1, the STL decreases at low frequencies when the niche exists compared to the baffled plate, Figure 4.23a. This discrepancy in STL continues up to $\frac{\omega}{\omega_c} = 0.54$ when $\lambda_{xy} \approx 2a$, then both systems have almost the same STL for the frequencies less than $\frac{\omega}{\omega_c} = 0.8$ when $\lambda_{xy} \approx 2b$, after that STL increases up to 2dB. The discrepancy diminishes where the acoustic wavelength is equal or less than $min\{a, b\}$, from this frequency ahead the niche effect is negligible. After that, the behaviour converges to the baffled plate behaviour.

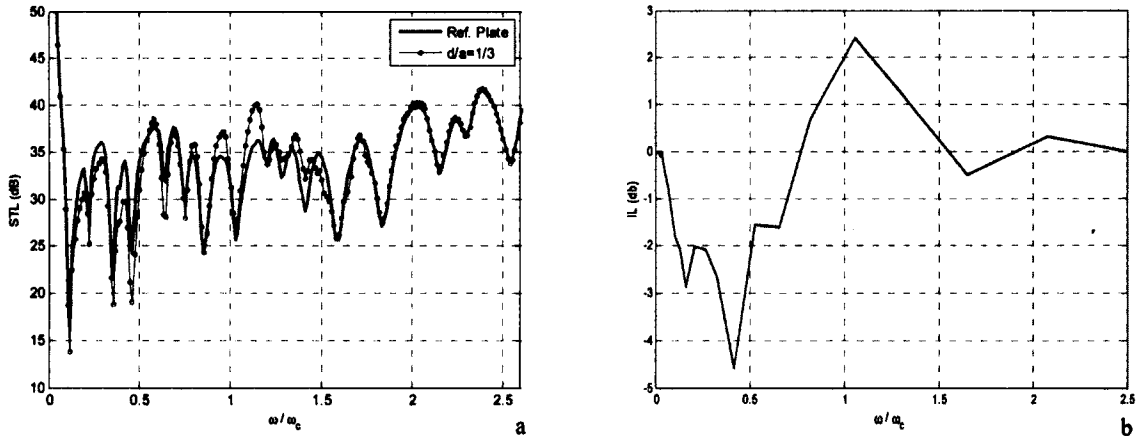

Figure 4.23: STL of the niche and plate, plate is placed at front side of the niche; a) Narrow band, b) 1/3 Octave band.

As mentioned before, the STL is dependent to the power transmitted and incident power. Unlike the baffled plate, the power transmitted through plate-niche at low frequencies is more than power transmitted through baffled plate. Since the excitation is the same and fluid

loading is small, the average mean square velocity of the plate remains the same as the baffled plate, Figure 4.24. So niche doesn't have effects on vibration field when it placed at back side of the plate.

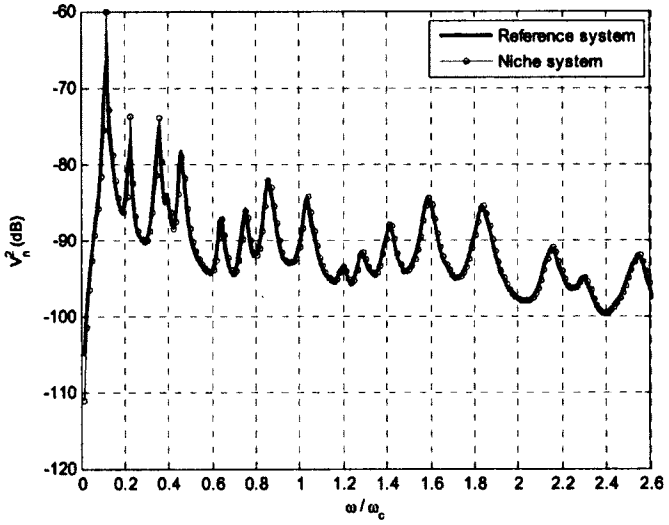

Figure 4.24: Average mean square velocity. plate is placed at front side of the niche.

So, the radiation efficiency of the system, equation 4.69, depends on power radiated by the plate inside the niche when the plate is located inside the niche which parenthetically is the same as the power radiated by the aperture if there is no damping in the niche cavity as shown in Figure 4.25, niche amplifies the radiation efficiency (the niche modal behavior is clearly seen in the radiation efficiency).

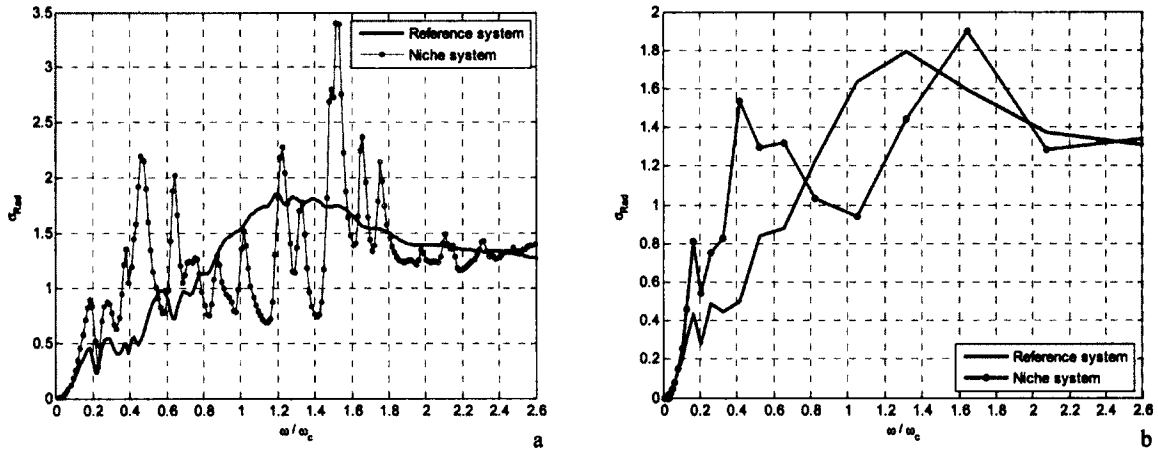

Figure 4.25: Effect of niche on radiation efficiency. plate is placed at front side of the niche; a) Narrow band, b) 1/3 Octave band.

4.5.4 Effect of niche-depth on radiation

STL of the system differs when the niche-depth changes, this effect is shown in Figure 4.26. The STL decreases as the length of the niche increase. For the case in which $\frac{d}{a} = \frac{1}{6}$, the STL decreases up to 2 dB before critical frequency. But, the STL falls to three times when the niche depth doubled and up to four times when niche depth is tripled, Figure 4.27. After that, STL improves, but the difference is less than 1 dB. Niche effect vanishes when the acoustic wave length in z direction is smaller than niche length. The effect of niche depth on radiation efficiency of the plate is shown in Figure 4.28. As shown in this figure, the radiation efficiency of the plate increases for the longer niche for the frequencies $\omega/\omega_c < 0.5$.

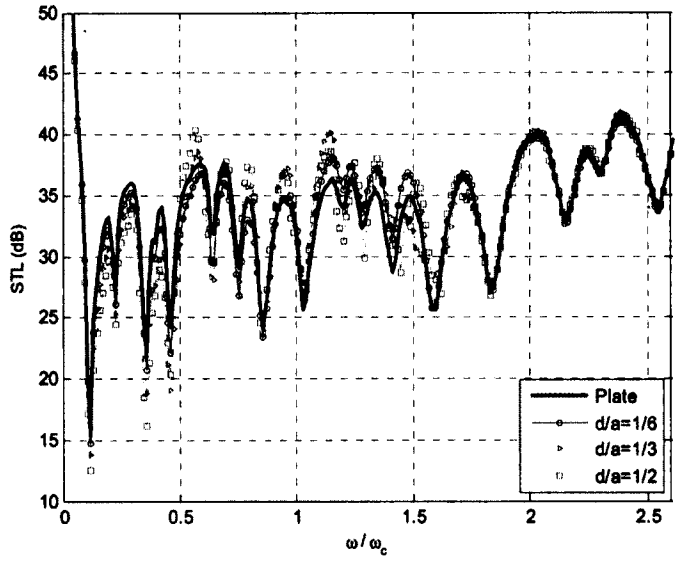

Figure 4.26: Niche depth effect on STL when plate is at front side of the niche.

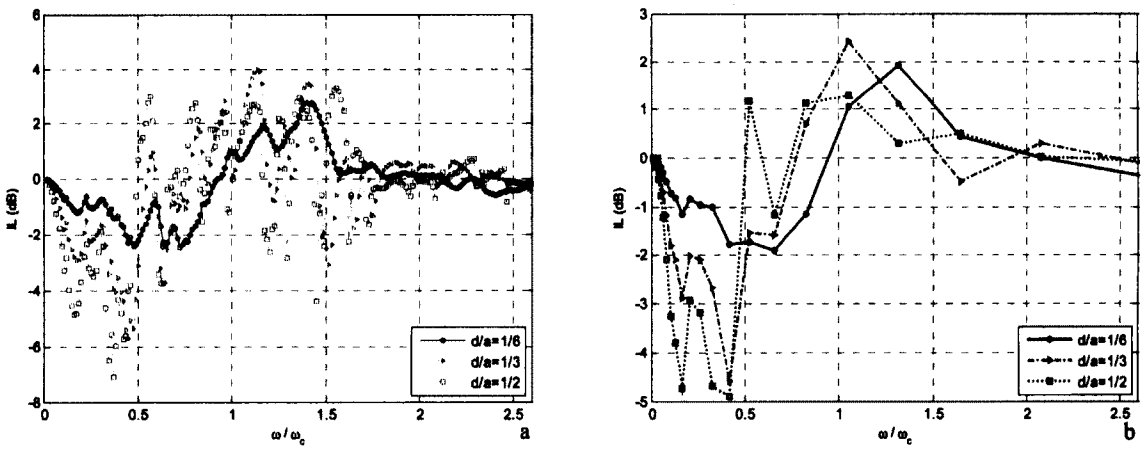

Figure 4.27: Effect of niche length on niche effect frequency range; a) Narrow band, b) 1/3 Octave band.

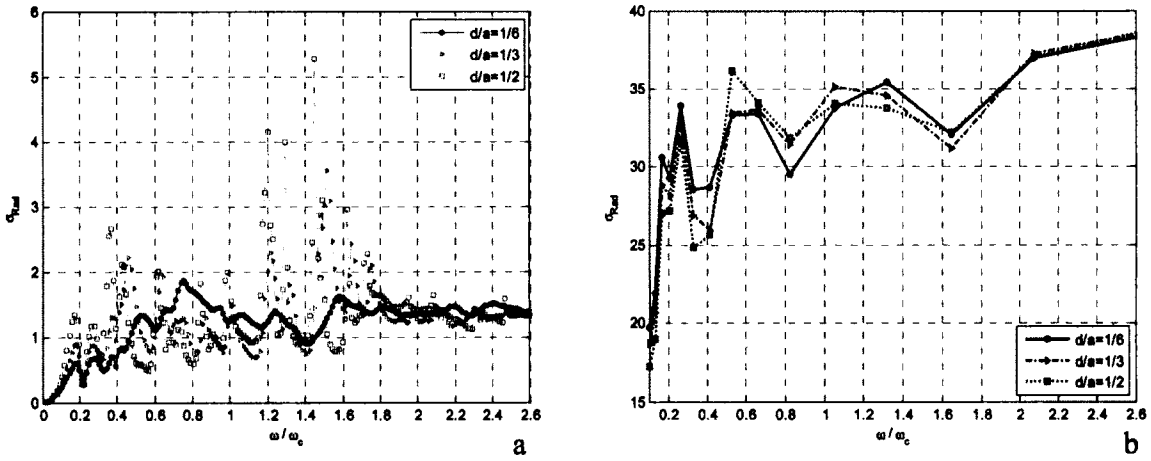

Figure 4.28: Effect of niche depth on radiation efficiency of the plate which is placed at front side of the niche; a) Narrow band, b) 1/3 Octave band.

4.5.5 The effect of plate position inside the niche on STL

The effect of niche on excitation and radiation is studied in previous sections, separately. Niche affects both the excitation and radiation fields, when plate is placed inside the niche, Figure 4.29. These effects for different plate position will be investigated in this section.

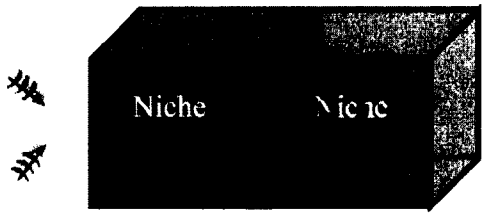

Figure 4.29:Niche affects both exciting and rcieving side.

To show the plate position inside the niche a normalized number which is the ratio of plate position over depth, $\xi = z_p/d$, is defined. Plane wave excitation is considered, Table 4.4 and the niche depth ratio is $d/a = 1/3$. Effect of plate position in five points, $= 0, \xi = 0.2, \xi = 0.5$, $\xi = 0.7$ *and* $\xi = 1.0$, is shown in Figure 4.30 and Figure 4.31. It is observed that, the STL decreases for all the frequency before critical frequency.

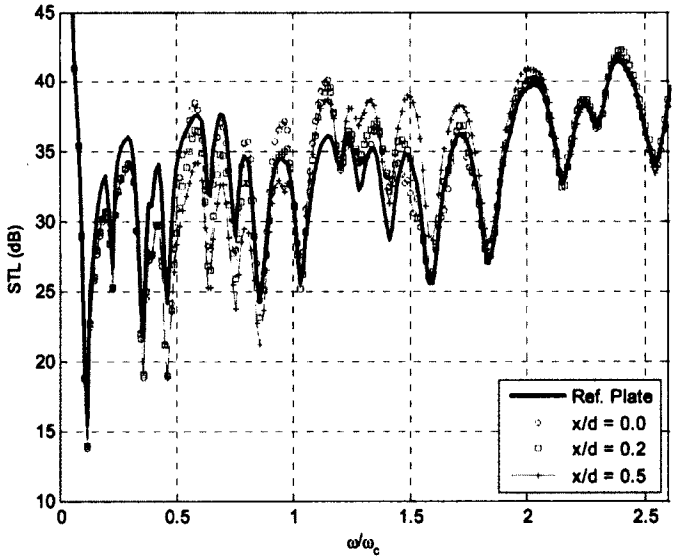

Figure 4.30: Effect of plate position on STL.

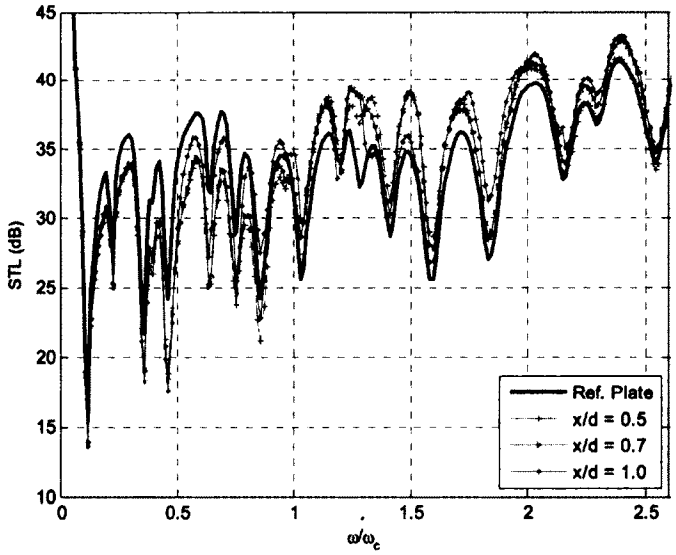

Figure 4.31: Effect of plate position on STL.

Niche effect is minimum when the plate is flushed mounted with front or back side of the niche, $\xi = 0$ and $\xi = 1$. The STL reduces significantly when the plate placed at the center of the niche. Comparing these results confirms that niche affects the excitation field more than radiation field, Figure 4.32. By changing the plate position inside the niche, from $\xi = 0$ to $\xi = 1$, the effect of niche on radiation reduces and the effect of niche on excitation increases.

For $\xi = 0.5$, the effect on radiation and excitation is the same. Equal volumes of niches at both sides of transmitting panel increase the transmission of energy through the panel especially at eigen-modes, Figure 4.32. Because of change in excitation field inside the niche, the effect of plate position inside the niche becomes noticeable when $1.5 \geq \frac{\omega}{\omega_c} \geq 0.5$. The effect of plate position inside the niche at different frequencies is shown in Figure 4.33. Niche effect can be reduced by placing the plate in front side of the niche, as shown in Figure 4.33 b.

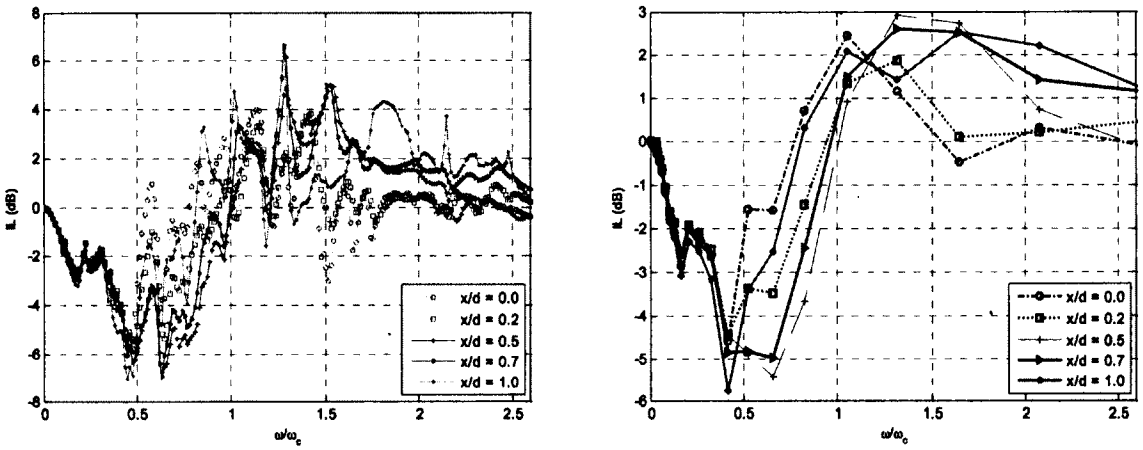

Figure 4.32: Effect of plate position on niche effect; a) Narrow band, b) 1/3 Octave band.

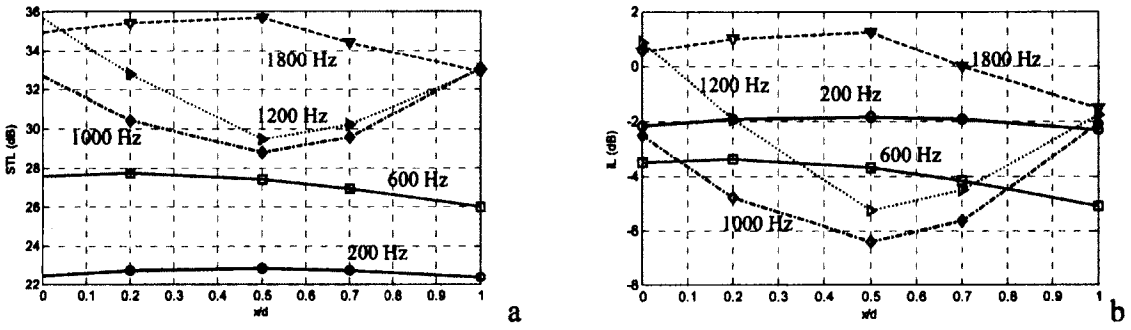

Figure 4.33: Effec of plate position inside the niche at different frequencies; a) STL, b) IL.

4.5.6 The effect of niche depth on STL

Effect of niche depth on STL when plate is placed at front side or back side of the niche was investigated in sections 4.5.2 and 4.5.4, respectively. This effect when plate is placed at the center of the niche is shown from Figure 4.34. STL decreases up to 2.5 dB when depth-ratio is $\frac{d}{a} = \frac{1}{6}$, this growth continues up to 7dB and 10 dB while depth increase to $\frac{d}{a} = \frac{1}{3}$ and $\frac{d}{a} = \frac{1}{2}$, Figure 4.34 and Figure 4.35. The diminution is more than when the plate is flush mounted with one side of the niche. In addition, improvement in STL begins at lower frequency for deeper niche and it goes up to 8 dB when $\lambda_z/d = 1$ for each depth.

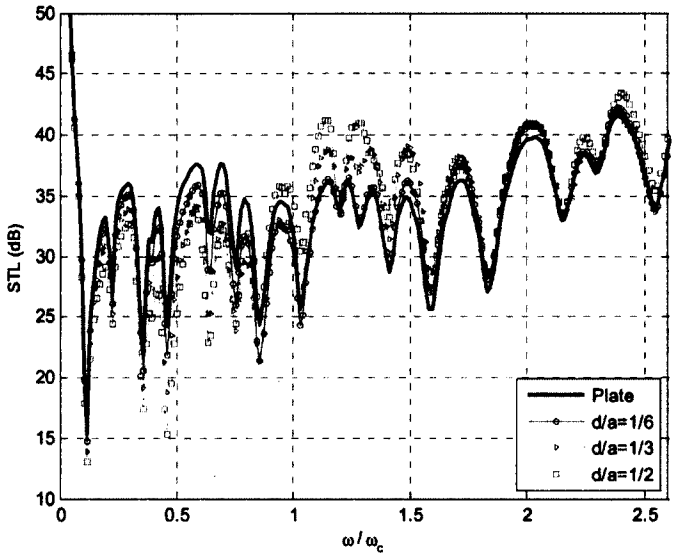

Figure 4.34 : Effect of niche depth on STL.

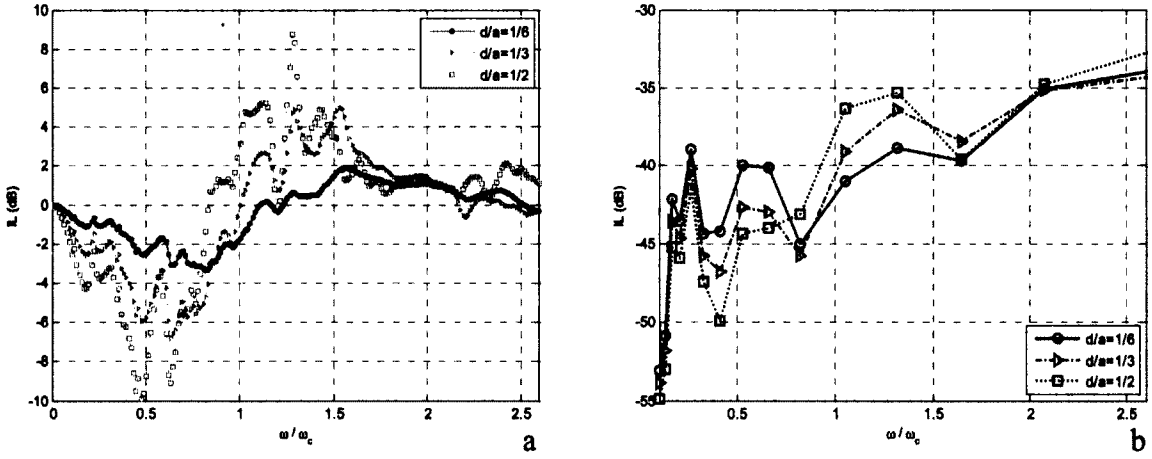

Figure 4.35: Effect of niche depth on STL; a) Narrow band, b) 1/3 Octave band.

The effect of diffuse acoustic field on niche when plate is placed at the center of the niche, is shown in Figure 4.36. In this case, the plate is placed inside the niche at $\frac{x}{d} = \frac{1}{2}$. The geometry and physical property of niche are mentioned in Table 4.1, Table 4.2 and Table 4.3. The depth-ratio of the niche is $\frac{d}{a} = \frac{1}{3}$. System is excited by diffuse acoustic excitation; number of plane waves and amplitude are given in Table 4.4. It can be observed that the STL in diffuse acoustic field is equal or lees than STL in plane wave excitation.

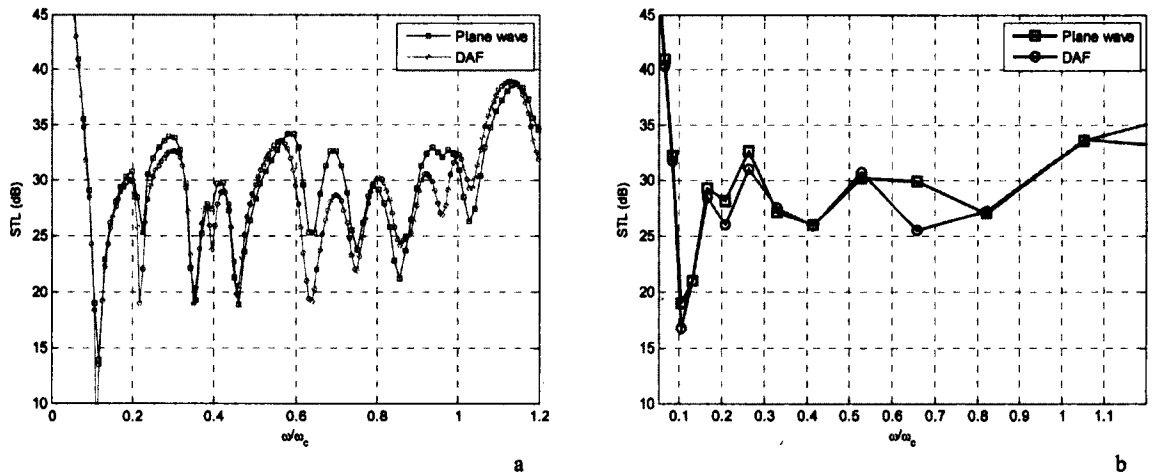

Figure 4.36: Niche effect. The length of the niche is d/a=1/3, plate placed at x/d=1/2; a) Narrow band, b) 1/3 Octave band.

4.6 Summary

The method proposed in chapter three is adapted in this chapter for the case where a plate is installed inside the niche. Results of niche effects on excitation and radiation fields show that niche affects the excitation field by increasing the pressure over the plate. This increase of pressure is more considerable at corners and edges of the plate. The influence becomes more significant as niche depth increases. This increase in vibration field causes more power be transmitted. So, the STL decreases. It continues up to the frequency where $\lambda_{xy} = a$. In contrast, when plate is placed at front side of the niche, the excitation field remains the same as for the baffled plate. In this case, STL decreases due to increase in radiation efficiency of the plate. For the same position of the plate, STL decreases at low frequencies up to 2dB, 4 dB and 6dB by increasing the depth to size ratio (d/a) from $1/6$ to $1/3$ and to $1/2$ for the frequencies below $\omega/\omega_c < 0.5$. Niche effect diminishes when the acoustic wave length becomes smaller than niche depth. Overall our study reveals niche has more effect on excitation field than radiation field. Effect of plate position inside the niche is investigated and at low frequencies minimal STL obtained when the plate is placed at the center of the niche. These results for specimen location are confirmed by (Cops, et al., 1987), experimentally. The studies of (Kim, et al., 2004) show that the sound transmission, when plate is placed at the center, increases. In this case, niche affects both exciting and radiation fields and because of symmetry maximum power transmission happens at this position. Consequently the niche effect is less considerable when plate is placed at front side of the niche.

CHAPTER 5 CONCLUSION AND PERSPECTIVES

5.1 Conclusion

Literature review shows significant differences in measurement of the sound transmission loss of the niche. These results demonstrate that for the same niche system, different STLs from different laboratories are obtained.

Developing a powerful, durable and fast semi-analytical tool to investigate niche effects on STL, compared to FEM-BEM, numerical tool is introduced as objective of this work. First, the model for predicting the STL of an aperture is presented. Then the model is extended for niche-plate system and niche parameters effects on STL are studied.

In this work, the semi-analytical method to study sound transmission loss of baffled aperture of rectangular cross section is presented. The acoustic waves inside the aperture are expanded according to evanescent and propagating acoustical modes. Aperture effect is studied for both plane wave and diffuse acoustic waves. Findings show that, the difference between diffuse acoustic field and plane wave excitation for same aperture depth is less than 1 dB in all frequency range. In addition, 60% decrease in transmitted power was observed when the length of the niche was doubles. Moreover, increasing in aperture depth can modify STL more considerably than reducing the cross section area.

The method is next extended for the case where a plate is placed inside the niche. Niche effect on excitation is investigated by placing the plate at the receiver end of the niche. Niche causes increase in pressure over the plate especially at corners and edges of the plate. The influence becomes more significant as niche depth increases. Change in excitation field origins more transmitted power. So, the STL decreases. It continues up to the frequency where $\lambda_{xy}=a$. when niche affects the radiation field STL decreases due to increase in radiation efficiency of the plate which is in direct relation to the depth of the niche. Niche effect fades when the acoustic wave length becomes smaller than niche depth. Outcomes comparison reveals niche has more

effect on excitation field than radiation field. Effect of plate position inside the niche is investigated and minimal STL obtained when the plate is placed at the center of the niche. In this case, niche affects both exciting and radiation fields and because of symmetry maximal power transmission happens at this position. Consequently the niche effect is less considerable when plate is placed at front side of the niche.

5.2 Perspectives

Following topics are proposed to continue this study:

- The effect of placing several plates inside the niche on STL.
- Experimental tests in order to corroborate the predicted niche effect.
- Study the effect of adding a sound package on either side of the plate effect of damping.
- Study the niche effect for non-rectangular cross section.
- Develop a niche correction factor in order to correct the niche effect and find back the STL of the panel (see the work done by (Ohlrich & Hugin, 2004))

CONCLUSION EN FRANÇAIS

Dans ce travail nous avons étudié la perte par transmission acoustique d'une plaque mince installée dans un tunnel (niche) séparant deux milieux semi-infinis. Un modèle semi-analytique basé sur la méthode de Rayleigh-Ritz a été développé et valide numériquement par comparaison avec la méthode des éléments finis. Au-delà de la revue de la littérature, le travail s'est déroulé en deux phases. Dans la première, on considère le calcul de la perte par transmission d'une niche vide. Dans la deuxième phase, on a attaqué le problème de la perte par transmission sous champ diffus d'une plaque placée à l'intérieur de la niche. Le problème et ses conditions de couplages ont été formulés mathématiquement.

Une approche de Ritz est utilisée ensuite pour décrire le champ déplacement normal de plaque (supposée mince et simplement appuyée) et les champs de pressions dans les deux cavités, de part et d'autre de la plaque. Ces dernières sont supposées a parois rigide et couplée chacune a son extermine avec un milieu semi-infini. Les couplages intermodaux et fluide-structure (impédances de rayonnement des cotes émission et réception) sont bien pris en compte. La validation du modèle est faite par comparaison avec la méthode des éléments finis (NOVAFEM). Finalement, une étude paramétrique pour expliquer la physique du problème et dégager des conclusions d'intérêt pratique est proposée.

Les découvertes montrent une décroissance considérable dans la puissance transmise lorsque la longueur de niche augmente. De plus, la longueur de niche joue un rôle important dans la transmission sonore comparée à la surface de section transverse de celle-ci. Dans le système niche-plaque, la niche affecte le champ d'excitation en augmentant la pression sur la plaque. L'augmentation de pression est plus importante au niveau des angles et des arêtes de la plaque. Nos résultats d'étude révèlent que la niche a plus d'effet sur le champ d'excitation que sur le champ de radiation. Ceci est important pour les essais expérimentaux où le champ source est mesuré dans une chambre réverbérant. Un minimum de perte par transmission sonore, en comparaison avec d'autres positions de plaque dans la niche, est obtenu lorsque la plaque est située au centre de la niche. Par conséquent, l'effet de niche est moins important quand la plaque est située dès le début de la niche.

APPENDIX A NORMAL DIRECTION FOR RAYLEIGH INTEGRAL

The normal direction of Rayleigh integral is shown by "*n*" in following figure. The normal n_1 is assumed in the equation.

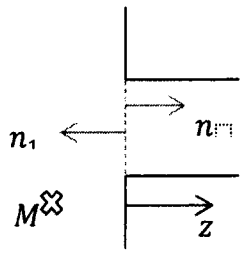

Normal direction for Rayleigh Integral

$$p_r(M) = \int_s G(M, M_0) \frac{\partial p_r}{\partial n}(M_0) ds(M_0)$$

$$\frac{\partial p_r}{\partial n} = -\frac{\partial p_r}{\partial n_1}$$

$$p_r(M) = -\int_s G(M, M_0) \frac{\partial p_r}{\partial n_1}(M_0) ds(M_0)$$

$$\frac{\partial p_r}{\partial n_1} = \nabla p . n_1 = n_1^T . \nabla p = [0\ 0\ -1] \begin{Bmatrix} p_{,x} \\ p_{,y} \\ p_{,z} \end{Bmatrix} = -p_{,z}$$

Then:

$$p_r(M) = \int_s G(M, M_0) \frac{\partial p_r}{\partial z}(M_0) ds$$

For the receiving side:

$$\frac{\partial p_r}{\partial n_1} = \nabla p . n_1 = n_1^T . \nabla p = [0\ 0\ 1] \begin{Bmatrix} p_{,x} \\ p_{,y} \\ p_{,z} \end{Bmatrix} = p_{,z}$$

So,

$$p_r(M) = -\int_s G(M, M_0) \frac{\partial p_r}{\partial z}(M_0) ds(M_0)$$

APPENDIX B IMPEDANCE INTEGRATION

The aperture cross modal radiation impedance between mode (p,q) and (u,v) is:

$$z_{uvpq} = j\rho\omega \int_{-b}^{b}\int_{-a}^{b}\int_{-b}^{b}\int_{-a}^{a} \varphi_{uv}(x,y)G(M,M_0)\varphi_{pq}(x_0,y_0)dxdydx_0dy_0$$

In order to calculate the integral, the following integral should be calculated:

$$I_{uvpq} = \int_{-1}^{1}\int_{-1}^{1}\int_{-1}^{1}\int_{-1}^{1} \varphi_{uv}(x',y')G(M',M'_0)\varphi_{pq}(x'_0,y'_0)dx'dy'dx'_0dy'_0$$

$$\varphi_{uv}(x',y') = \cos(\frac{p\pi(x'+1)}{2})\cos(\frac{q\pi(y'+1)}{2})$$

$$G(M,M_0) = \frac{e^{-jk_0l_xR/2}}{R}$$

Where,

$$R = \left[(x'-x'_0)^2 + \frac{(y'-y'_0)^2}{r^2}\right]^{1/2}$$

And

$$r = \frac{lx}{ly}$$

Finally Impedance is calculated as shown in the following:

$$z_{uvpq} = j\omega\rho(lxly^2/2\pi)I_{uvpq}$$

Where (S^2) comes from mapping of integral limits from [-a, a] to [-1, 1] and [-b, b] to [-1, 1]. To calculate I_{uvpq} according to the paper of (Nelisse, et al., 1997), by mapping the variables the integral will be as following:

$$I_{mnpq} = \int_0^2 \int_0^2 [G_{mp}(x) + G_{pm}(x)][H_{nq}(y) + H_{qn}(y)]k(x,y)\,dxdy$$

$$G_{mp}(\alpha) = \int_0^{2-\alpha} g_m(\alpha+\beta-1)g_p(\beta-1)d\beta$$

$$H_{nq}(\alpha) = \int_0^{2-\alpha} h_n(\alpha+\beta-1)h_q(\beta-1)d\beta$$

$$k(x,y) = \frac{e^{\frac{ikl_x}{2\left[x^2+\frac{y^2}{r^2}\right]^{\frac{1}{2}}}}}{\left[x^2+\frac{y^2}{r^2}\right]^{\frac{1}{2}}}$$

This Integral can be calculated by using Gauss quadrature method.

APPENDIX C COUPLING MATRIX

The coupling matrix in equation 4.32 is explained in this section.

$$\gamma_{uvmn} = \int_s \varphi_{uv}(x,y) \quad \Psi_{mn}(x,y)ds$$

By substituting φ_{uv} and Ψ_{mn} from equations 4.26,3.19, respectively, following integral should be solved:

$$\gamma_{uvmn} = \int_{-a}^{a} \sin\frac{m\pi(x+a)}{2a}\cos\left(\frac{p\pi(x+a)}{2a}\right)dx \int_{-b}^{b} \cos\left(\frac{q\pi(y+b)}{2b}\right)\sin\frac{n\pi(y+b)}{2b}dy$$

By defining and calculating the following integrals,

$$\boldsymbol{I_{mp}} = \int_{-a}^{a} \sin\frac{m\pi(x+a)}{2a}\cos\left(\frac{p\pi(x+a)}{2a}\right)dx$$

$$\boldsymbol{I_{qn}} = \int_{-b}^{b} \cos\left(\frac{q\pi(y+b)}{2b}\right)\sin\frac{n\pi(y+b)}{2b}dy$$

Finally:

$$\gamma_{uvmn} = \begin{cases} 0 & m = p \text{ or } n = q \\ \boldsymbol{I_{mp}} \times \boldsymbol{I_{qn}} & m \neq p \text{ and } n \neq q \end{cases}$$

LIST OF REFERENCES

Allard, J. F. & Atalla, N., 2009. *Propagation of Sound in Porous media Modelling Sound Absorbing Materials.* 2 ed. s.l.:John Wiley & Sons.

Atalla, N., 2011. Note of the Course GMC722 " Méthodes numériques en interaction fluide-structure". In: Sherbrooke: s.n.

Atalla, N. & Bernhard, R., 1994. Review of numerical solutions for low frequency structural acoustic problems. *Applied Acoustic,* 43(3), pp. 271-294.

Atalla, N., Nicolas, J. & Gauthier, C., 1996. Acoustic radiation of an unbaffled vibrating plate with general elastic boundary conditions. *Journal of the Acoustical Society of America,* 99(3), pp. 1484-1494.

Atalla, N., Panneton, R. & Debergue, P., 1998. A mixed displacement-pressure formulation for poroelastic materials. *Journal of the Acoustical Society of America,* 104(3), pp. 1444-1452.

Atalla, N., Sgard, F. & Amedin, K. C., 2006. On the modeling of sound radiation from poroelastic materials. *Journal of the Acoustical Society of America,* 120(4), pp. 1990-1995.

Bathe, 2006. *Finite Element procedure.* s.l.:Prentice Hall .

Chen, Roger, Mei & Chuh, 1995. *Finite element nonlinear random responce of composite plates to acoustic and thermal loads applied simultaneously.* s.l., s.n., pp. 1251-1261.

Cops, A., Minten, M. & Myncke, H., 1987. Influence of the design of transmission rooms on the sound transmission loss of glass- intensity versus conventional method. *Noise Control Engineering Journal,* 28(3), pp. 121-129.

Crags, A., 1971a. The transient response of a coupled plate-acoustic system using plate and acoustic finite elements. *Journal of Sound and Vibration,* 15(4), pp. 509-528.

Crags, A., 1972b. The use of simple three-dimensional acoustic finite elements for determining the natural modes and frequencies of complex shaped enclosures. *Journal of Sound and Vibration,* 23(3), pp. 331-339.

Dauchez, N., Sahraoui, S. & Atalla, N., 2001. Convergence of poroelastic finite elements based on Biot displacement formulation. *Journal of the Acoustical Society of America,* 109(1), pp. 33-40.

Dijckmans, A., Vermei, G. & Lauriks, W., 2010 b. Sound transmission through finite lightweight multilayered structures with thin air layers. *Journal of the Acoustical Society of America,* 128(6), pp. 3513-3524.

Dijckmans, A. & Vermeir, G., 2010 a. *A wave based model to describe the niche effect in sound transmission loss determination of single and double walls.* Sydney, Australia, Proceedings of 20th International Congress on Acoustics.

Dijckmans, A. & Vermeir, G., 2012. A wave based model to predict the niche effect on sound transmission loss of single and double walls. *Acta Acustica united with Acustica,* Volume 98, pp. 111-119.

Easwaran, V., Lauriks, W. & Coyette, J. P., 1996. Displacement-based finite element method for guided wave propagation problems: application to poroelastic media. *Journal of the Acoustical Society of America,* 100(5), pp. 2989- 3002.

Fahy, F. J. & Gardonio, P., 2007. *Sound and Structural Vibration, 2nd Edition.* s.l.:Academic Press.

Furue, Y., 1990. Sound Propagation from the Inside to the Outside of a Room Through an Aperture. *Applied Acoustic,* 31(1), pp. 133-146.

Gladwell, G., 1966. A variational formulation of damped acousto-structural vibration problems. *Journal of Sound and Vibration,* 4(2), pp. 172-186.

Göransson, P., 1995. A weighted residual formulation of the acoustic wave propagation through a flexible porous material and a comparison with a limp material model. *Journal of Sound and Vibration,* 182(3), pp. 479-494.

Halliwell, R. E. & Warnock, A. C. C., 1985. Sound transmission lost: comparison of conventional techniques with sound intensity techniques. *Journal of the Acoustical Society of America,* 77(6), pp. 2094-2103.

Hwang, C. & Pi, W., 1972. Nonlinear acoustic response analysis of plates using the finite element method. *AIAA Journal,* pp. 276-281.

Ji, Z. L. & Sha, J. Z., 1997. A boundary element approach to sound transmission/radiation problems. *Journal of Sound and Vibration,* 206(2), pp. 261-265.

Kim, B.-K.et al., 2004. Tunneling effect in sound transmission loss determination: Theoretical approach. *Journal of the Acoustical Society of America,* pp. 2100-2109.

Leppington, F., Broadbent, E. & Heron, k., 1982. The acoustic radiation efficiency of rectangular panels. *Proceedings of the Royal Society of london,* pp. 245-271.

Leppington, F. G., 1996. Acoustic radiation from plates into a wedge-shaped fluid region: application to the free plate problem. *Mathematical, Physical and Engineering Sciences,* Volume 452, pp. 1745-1764.

Leppington, F. G., Broadbent, E. G. & Heron, K. H., 1983. Acoustic radiation from rectangular panels with constrained edges. *Mathematical, Physical and Engineering Sciences,* Volume 393, pp. 67-84.

London, A., 1950. Transmission of reverberant sound through double walls. *Journal of the Acoustical Society of America,* 22(2), pp. 270-279.

Mattei, P. O., 1995. Sound radiation by baffled and costrained plates. *Journal of Sound and Vibration,* 179(1), pp. 63-77.

Nelisse, N., Beslin, O. & Nicolas, J., 1997. A generalized approach for the acoustic radiation from a baffled or un baffled plate with arbitrary boundary conditions, immersed in a light or heavy fluid. *Journal of Sounds and Vibration,* 211(2), pp. 207-225.

Ohlrich, M. & Hugin, C., 2004. On the influence of boundary constraints and angled baffle arrangements on sound radiation from rectangular plates. *Journal of Sound and Vibration,* Volume 277, pp. 405-418.

Panneton, R. & Atalla, N., 1996. Numerical prediction of sound transmission through finite multilayer systems with poroelastic materials. *Journal of the Acoustical Society of America,* 100(1), pp. 346- 354.

Panneton, R. & Atalla, N., 1997. An efficient finite element scheme for solving the three-dimensional poroelasticity problem in acoustics. *Journal of the Acoustical Society of America,* 101(6), pp. 3287- 3298.

Prosser, W., Hamstad, M., Gary, J. & O'Gallagher, A., 1998. Finite element and plate theory modeling of acoustic emission waveforms. *Journal of Nondestructive Evaluation,* pp. 83-90.

Rebillard, P. et al., 1992. The effect of a porous facing on the impedance and the absorption coefficient of a layer of porour materia. *Journal of Sound and Vibration,* 156(3), pp. 541-555.

Sauter, A. & Soroka, W. W., 1969. Sound Transmission through Rectangular Slots of Finite Depth between Reverberant Rooms. *Journal of the Acoustical Society of America,* 44(1), pp. 359-359.

Seybert, A., Soenarko, B., Rizo, F. & Shippy, D., 1985. An advanced computational method for radiation and scattering of acoustic waves in three dimensions. *Journal of the Acoustical Society of America,* 77(2), pp. 362-368.

Sgard, F., Nelisse, H. & Atalla, N., 2007. On the modeling of the diffuse field sound tranmission loss of finite thickness apertures. *Journal of the Acoustical Society of America,* 122(1), pp. 302 - 3013.

Silva, J. d. R., 1994. *Acoustic and elastic wave scattering using Boundary Elements.* Billerica, USA: Computational Mechanics.

Simon, B., Wu, J., Zienkiewicz, O. & Paul, D., 1986. Evaluation of u-w and u-pi finite element methods for the dynamic response of saturated porous media using one-dimensional models. *International Journal for Numerical & Analytical Methods in Geomechanics,* pp. 462-482.

Tournour, M. & Atalla, N., 1998. A novel acceleration method for the variational boundary element approach based on multipole expansion. *International Journal for Numerical Methods in Engineering,* 42(7), pp. 1199-1214.

Vinokur, R., 2006. Mechanism and calculation of the niche effect in airborne sound transmission. *Journal of the Acoustical Society of America,* 119(4), pp. 2211-2219.

Wilson, G. & Soroka, W. W., 1964. Approximation to the Diffraction of Sound by a Circular Aperture in a Rigid Wall of Finite Thickness. *Journal of the Acoustical Society of America,* 37(2), pp. 286-297.

Xuefeng, Z. & Wen, L. L., 2010. A unified approach for predicting sound radiation from baffled rectangular plates with arbitrary boundary conditions. *Journal of Sound and Vibration,* Volume 329, pp. 5307-5320.

Yoo, J. W., 2010. Study on the general characteristics of the sound radiation of a rectangular plate with different boundary edge conditions. *Journal of Mechanical Science and Technology,* 25(4), pp. 1111-1118.

Yufeng, Q. & Qibai, H., 2006. The effect of boundary conditions on sound loudness radiated from rectangular plates. *Archive of Applied Mechanics,* Volume 77, pp. 21-34.

Zienkiewicz, O. & Taylor, R., 2000. *The finite element method.* s.l.:Butterworth-Heinemann.